NATURAL RESOURCES

GEOLOGIC MAP OF THE ELLENSBURG NORTH AND SOUTHERN HALF OF THE REECER CANYON 7.5-MINUTE QUADRANGLES, KITTITAS COUNTY, WASHINGTON

by Andrew J. Sadowski, J. Bodie McCosby, Megan L. Anderson, Todd R. Lau, Ashley Steiner, S. Andrew DuFrane, Tammy Rittenour, and Bernard Housen

WASHINGTON
GEOLOGICAL SURVEY
Map Series 2020-01
December 2020

INTERNALLY REVIEWED

WASHINGTON STATE DEPARTMENT OF
NATURAL RESOURCES
WASHINGTON GEOLOGICAL SURVEY

GEOLOGIC MAP OF THE ELLENSBURG NORTH AND SOUTHERN HALF OF THE REECER CANYON 7.5-MINUTE QUADRANGLES, KITTITAS COUNTY, WASHINGTON

by Andrew J. Sadowski, J. Bodie McCosby, Megan L. Anderson, Todd R. Lau, Ashley Steiner, S. Andrew DuFrane, Tammy Rittenour, and Bernard Housen

WASHINGTON
GEOLOGICAL SURVEY
Map Series 2020-01
December 2020

This geologic map was funded in part by the USGS National Cooperative Geologic Mapping Program, award no. G19AC00220

This publication has been subject to an iterative technical review process by at least one Survey geologist who is not an author. This publication has also been subject to an iterative review process with Survey editors and cartographers.

WASHINGTON STATE DEPARTMENT OF
NATURAL RESOURCES
WASHINGTON GEOLOGICAL SURVEY

DISCLAIMER

INDEMNIFICATION

Research supported by the U.S. Geological Survey, National Cooperative Geologic Mapping Program, under USGS award number G19AC00220. The views and conclusions contained in this document are those of the authors and should not be interpreted as necessarily representing the official policies, either expressed or implied, of the U.S. Government.

WASHINGTON STATE DEPARTMENT OF NATURAL RESOURCES

WASHINGTON GEOLOGICAL SURVEY

Washington State Department of Natural Resources
Washington Geological Survey

Mailing Address:
MS 47007
Olympia, WA 98504-7007

Street Address:
Natural Resources Bldg, Rm 148
1111 Washington St SE
Olympia, WA 98501

Phone: 360-902-1450
Fax: 360-902-1785
Email: geology@dnr.wa.gov
Website: http://www.dnr.wa.gov/geology

Publications and Maps:
www.dnr.wa.gov/programs-and-services/geology/publications-and-data/publications-and-maps

Washington Geology Library Searchable Catalog:
www.dnr.wa.gov/programs-and-services/geology/washington-geology-library

Suggested Citation: Sadowski, A. J.; McCosby, J. B.; Anderson, M. L.; Lau, T. R.; Steiner, Ashley; DuFrane, S. A.; Rittenour, Tammy; Housen, Bernard, 2020, Geologic map of the Ellensburg North and southern half of the Reecer Canyon 7.5-minute quadrangles, Kittitas County, Washington: Washington Geological Survey Map Series 2020-01, 1 sheet, scale 1:24,000, 25 p. text. [http://www.dnr.wa.gov/publications/ger_ms2020-01_geol_map_ellensburg_north_reecer_canyon_24k.zip]

Contents

FIGURES

MAP SHEET

Geologic Map of the Ellensburg North and Southern Half of the Reecer Canyon 7.5-minute Quadrangles, Kittitas County, Washington

by Andrew J. Sadowski[1], J. Bodie McCosby[1], Megan L. Anderson[1], Todd R. Lau[1], S. Andrew DuFrane[2], Ashley Steiner[3], Tammy Rittenour[4], Bernard Housen[5]

[1] Washington Geological Survey
MS 47007
Olympia, WA
98504-7007

[2] Department of Earth and Atmospheric Sciences
University of Alberta
1-26 Earth Sciences Building
Edmonton, Alberta
Canada T6G 2E3

[3] Peter Hooper GeoAnalytical Lab
School of the Environment
Washington State University
Webster 1228
Pullman, WA
99164-2812

[4] Luminescence Laboratory
Utah State University
1770 North Research Parkway
Suite 123
North Logan, UT
84341-1844

[5] Pacific Northwest Paleomagnetism Laboratory
Geology Department
Western Washington University
16 High St.
Bellingham, WA
98225-9080

ABSTRACT

New geological and geophysical investigations of the Ellensburg North and Reecer Canyon quadrangles characterize geologic structures of the northwestern Yakima fold and thrust belt and the basin architecture of Kittitas Valley. New 1:24,000-scale mapping identifies south-verging, reverse-to-thrust faults with short-hinged anticlines and synclines, long-hinged monoclines, and north-northeast- and north-northwest-oriented strike-slip faults. Forward modeling of gravity and aeromagnetic data constrains our interpretations of fault and fold geometries and suggests thickness variations on the order of hundreds of meters in Miocene basalts, thinning of Eocene sedimentary rocks, and shallowing of basement rocks northward.

Our mapping refines bedrock and surficial stratigraphy near the northern extent of the Miocene Columbia River Basalt Group (CRBG). Novel machine learning techniques using whole rock geochemistry newly identify the Wapshilla Ridge, Grouse Creek, Ortley, and Sentinel Bluffs members of Grande Ronde Basalt (GRB of CRBG) within the map area. The Coleman member of the sedimentary Ellensburg Formation divides the Grouse Creek member and its hyaloclastite facies from younger GRB members. New detrital zircon U-Pb analyses from two pumiceous siltstones—one above and one below the Coleman member—indicate a ~16.0 Ma maximum depositional age. Lidar-informed mapping of unconsolidated surficial deposits combined with new Pliocene through Holocene U-Pb and luminescence ages delineates intermingling of Cascade-sourced alpine glacial outwash and locally sourced alluvium that cap older bedrock.

Lidar derivatives improved identification of landslides and young fault escarpments. The Coleman member and other interbeds highlight areas prone to landslides at the surface and suggest zones of potential aquifers at depth. Basalt is shallowly concealed (>2 ft) north of the Dead Coyote fault and may support shallow recharge potential for deeper aquifers.

INTRODUCTION

The Ellensburg North and southern half of the Reecer Canyon 7.5-minute quadrangles (herein also referred to as "the map area") are located in east-central Kittitas County, Washington. They cover the northern portion of Kittitas Valley in central Washington on the western edge of the Columbia Basin and east of the Cascade Range. Much of the map area near the Yakima River and the city of Ellensburg is developed for commercial, industrial, and residential uses, whereas areas north of the city are cultivated for agriculture. Higher elevations are a mix of private residential land and the Wenatchee National Forest. Numerous active and inactive rock quarries are scattered throughout the map area.

To better understand geologic hazards (seismic, landslide, debris flow) and natural resources (water, aggregate), our 1:24,000-scale geologic map builds upon prior geologic mapping at 1:100,000 scale (Waitt, 1979; Tabor and others, 1982) and at 1:24,000 scale (Rosenmeier, 1968). Our mapping also identifies stratigraphy very similar to detailed geologic mapping by Hammond (2013) southwest of the map area near the Naches River. Our work is part of a multi-year geologic mapping effort to characterize Puget Lowland active faults in the broader tectonic context that ranges from the Yakima fold and thrust belt (YFTB) to the Cascade Range. New and ongoing work aims to better characterize faults and deformation from eastern Washington to western Washington. The mapping will

assist in geologic hazard assessment, geotechnical engineering, groundwater hydrology, earth resource management, academic research, and investigations for growth management planning.

GEOLOGIC OVERVIEW

Bedrock

The oldest rocks exposed in the map area are basaltic andesite of the Miocene Grande Ronde Basalt (GRB) of the Columbia River Basalt Group (CRBG), a continental flood basalt province (Reidel and Tolan, 2013). Roughly 95 percent of the CRBG erupted rapidly between 16.7 and 15.9 Ma (Kasbohm and Schoene, 2018). The GRB constitutes ~72 percent of the CRBG formations by volume (Reidel and others, 2013a). The oldest exposed GRB member is the Wapshilla Ridge Member, located in Wilson Creek and northwest of the map area, whereas the youngest exposed GRB member is the Sentinel Bluffs Member, located near Table Mountain in the northern map area and south of the range front in Kittitas Valley.

Volcaniclastic and feldspathic sedimentary rocks of the Ellensburg Formation overlie, interfinger, and underlie the GRB (Schmincke, 1964, 1967; Smith, 1988a, 1988b). The ancestral Cascade Range provided volcaniclastic detritus to the ancestral Columbia Basin, whereas the feldspathic material in the basin is sourced from ancient rivers of the inland Pacific Northwest (such as the ancestral Columbia River; Schmincke, 1964, 1967; Smith 1988a, 1988b). A notable horizon within the Ellensburg Formation is the Coleman member—informally named by Bentley (1977)—and identified in Coleman Canyon east of the map area. The Coleman member of the Ellensburg Formation is an extensive, micaceous interbed that overlies the Grouse Creek member and underlies the Sentinel Bluffs Member.

Surficial Deposits

Miocene bedrock is unconformably capped by Pliocene through Holocene glacial and nonglacial deposits. Glacial deposits are related to alpine glaciations in the Cascade Range. Porter (1976) and Waitt (1979) mapped glacial and glaciofluvial deposits in detail to the west of and within the map area, respectively. A sequence of Pliocene through Holocene glacial outwash trains records three drifts (Waitt, 1979) with at least two provenances: polymict and Cascade-sourced versus monomict and locally sourced basalt. In the map area, these drifts include, from oldest to youngest: 1) Thorp Gravel; 2) Kittitas Drift with its Swauk Prairie and Indian John phases; and 3) Lakedale Drift with its Bullfrog Member. When clear evidence for alpine ice was lacking, we mapped alluvial deposits as possible glaciofluvial units.

Previous investigations reported two generalized sources of alpine glacial outwash that exist in the map area: mainstream and side stream. The work of Porter (1976) and references therein firmly established the Yakima River corridor as a source of mainstream alpine glacial outwash from the Cascade Range. Waitt (1979) presented examples of side stream glacial alpine outwash deposits which originated from northern canyons of Kittitas Valley. Mainstream outwash comes from the Cascade Range while side stream outwash comes from adjacent canyons. In the adjacent quadrangle to the west, Green Canyon represents an unambiguous side stream corridor that channeled alpine outwash southward into the map area (Waitt, 1979). Possible side stream corridors in the map area may include, from west to east: Johnson, Reecer, Robbins, Currier, Snag, Wilson, and Naneum Canyons, but evidence for glacial ice in their respective headwaters is not clear. Additional work is recommended in the northern half of the Reecer Canyon quadrangle and areas north and west to assess these questions. Our work avoids the mainstream/side stream nomenclature in favor of grouping these facies. We divide the outwash terraces based on relative ages inferred from differences in elevation and surface morphologies using new lidar data, not based solely by provenance. These differences delineate glacial outwash, alluvial fans, and terrace-to-overbank deposits.

Glacial and alluvial unconsolidated deposits were later blanketed by Pleistocene eolian loess of the Palouse Formation across central and eastern Washington. The sediment source for loess was the wind-blown redistribution of fine-grained sand and silt of slackwater deposits from cataclysmic floods related to continental glaciations (McDonald and Busacca, 1992). Landslide deposits and mass-wasting landforms drape older units and are identified using field- and lidar-informed observations.

Tectonic Framework

The map area lies within the modern backarc of the Cascadia subduction zone. During the Paleogene, extensional and transtensional structural basins filled with nonmarine Eocene sediments and volcanic rocks (Tabor and others, 1982; Johnson, 1985; Eddy and others, 2016, 2017). These continental basins were later filled and capped by voluminous Neogene lavas at least during the onset of Miocene compression and transpression. This stress regime resulted from oblique subduction with concomitant steady regional clockwise rotation (Wells and McCaffrey, 2013; Brocher and others, 2017). GPS velocities show ongoing north-northeast-directed shortening (McCaffrey and others, 2013; Wells and others, 1998). Deformation is accommodated by extensive kilometer-scale, west- and northwest-striking, reverse-to-thrust faulting with associated folds that produced the Yakima fold and thrust belt (YFTB; Reidel and others, 2013b; Kelsey and others, 2017; Staisch and others, 2018a,b). The map area encompasses the northern extent of the YFTB from Kittitas Valley to the Wenatchee Mountains (Rosenmeier, 1968; Tabor and others, 1982). Miocene units are subhorizontal and flat-lying in the Wenatchee Mountains to the north, and are tilted progressively southward toward Kittitas Valley.

METHODS

Geologic Mapping

We identified lithologic units from field observations in the summer and fall of 2019. Field data were collected using traditional geological field methods and digitally recorded in the field with Esri's ArcGIS Collector application. The geologic map was refined using prior geologic mapping at 1:100,000-scale (Waitt, 1979; Tabor and others, 1982) and 1:24,000-scale (Rosenmeier, 1968), recent aerial orthophotos, and elevation data from lidar (UNAVCO, 2008; Yakima Nation, 2010; FEMA, 2011; Kittitas

County, 2012; WA DNR, 2014, 2018a,b; PSLC/WA DNR, 2015). Lidar data were used to derive hillshade images, contours, red relief image maps (Chiba and others, 2008), and other terrain products. Bedding attitudes, sedimentary structure, igneous foliation, joints, and shears in bedrock were measured where the feature did not appear to be a randomly oriented crack or brecciation of unknown origin. In CRBG rocks, vesicular tops and tops of colonnade were measured to provide orientations of flow foliation surfaces. Similarly, the orientations of column sides in colonnade sections were also measured and analyzed sterographically using Stereonet 10.1.0 software (Allmendinger and others, 2012; Cardozo and Allmendinger, 2013) to verify cooling surfaces inferred to represent paleo-horizontal.

Data Collection and Analysis

We reviewed multiple datasets, including well logs, boring records, geotechnical reports, geophysical data (gravity and aeromagnetics), fluxgate magnetometry for magnetostratigraphy, geochemical analyses (major element and trace element), petrographic analysis of thin sections, clast counts for sedimentary provenance, and identification of geomorphic features using lidar. More than 80 water wells, geotechnical borings, and oil and gas wells were reviewed to inform subsurface understanding.

POTENTIAL-FIELDS GEOPHYSICAL METHODS

New gravity data were collected using a Scintrex model CG-6 gravimeter. Grid spacing was 1–2 km (3,281–6,562 ft) with profile lines at 250-m (820 ft) spacing. Gravity data are referenced to the International Gravity Standardization Net of 1971 (Morelli, 1974). Isostatic anomalies result from applying Bouguer, Earth curvature, and terrain corrections to 166.7 km using the standard reduction density of 2,670 kg/m^3, a 25-km-thick crust at sea level and a crust-mantle density contrast of 400 kg/m^3 (Heiskanen and Vening-Meinesz, 1958; Jachens and Roberts, 1981; Telford and others, 1976; Swick, 1942). A horizontal gradient filter applied to the isostatic gravity grid helped identify linear gravitational gradients, commonly associated with steeply dipping contacts or with faults, where stronger gradients usually imply more extreme deformation. Aeromagnetic data from two surveys (Blakely and others, 2020a,b) identify magnetic anomalies related to volcanic bedrock and highlight lineaments possibly related to faults or folds.

Forward modeling of the potential-field anomalies along Cross Section A–A′ using GM-SYS (Geosoft, Inc.) helped constrain possible bedrock geometries in the subsurface. In addition to published rock properties (Staisch and others, 2018a,b), more than 30 density and magnetic susceptibility measurements from samples collected throughout the map area provide guidance for our modeling parameters for local units. Well W28 also provides the approximate minimum depth of basalt under Kittitas Valley (Figure M1B). CRBG thicknesses and the top of CRBG within Kittitas Valley at the southern end of our model agree with models by Staisch and others (2018a) and Kelsey and others (2017) in nearby areas.

Fluxgate Magnetometry

A portable fluxgate magnetometer was used to assess the polarity of whole rock magnetization—reverse or normal—for members of the CRBG (see *Appendix A* for details). We analyzed 37 sites to compare our mapping to the magnetostratigraphy of previous mapping by Tabor and others (1982), and to understand what magnetostratigraphic unit of the GRB we were in. Notably, some of our fluxgate readings—and portions of the aeromagnetic data—disagree with magnetostratigraphy of prior GRB mapping (Tabor and others, 1982).

GEOCHEMISTRY

A total of 54 samples were selected for whole rock major and trace element analysis and analyzed at the Peter Hooper GeoAnalytical Laboratory at Washington State University. Major element compositions were measured using X-ray fluorescence (XRF) via inductively coupled plasma atomic emission spectroscopy (ICP-AES) and trace element compositions were measured using inductively coupled plasma mass spectroscopy (ICP-MS) (Data Supplement Table DS01). Geochemical analyses of samples from the crystalline cores of lavas (colonnades and entablatures) were preferred for analysis because they give more representative compositional results. If neither were available, then sampes from vesicular tops sufficed, with a caveat being that geochemistry from the oxidizing cooling surface of a lava flow may be geochemically less representative than the core of the flow. Note that geochemistry sites G01–06 reside outside of the map area.

Geochronology

U-PB ANALYSIS OF DETRITAL ZIRCON GRAINS

U-Pb analysis of detrital zircon grains extracted from six samples in the map area provide new information about sediment provenance and depositional age for units within the Ellensburg Formation and sediments of Pliocene gravels ("Naneum Gravel" unit QRcg; Data Supplement DS02). Detailed methodology can be found in the Data Supplement (Table DS02). Four ages came from the Ellensburg Formation: one from a sedimentary rock below the Coleman member (unit Mcf$_e$, age site GD01), one from the Coleman member (unit Mcs$_{ec}$, age site GD02), one from a sedimentary rock above the Coleman member (unit Mcf$_e$, age site GD03), and one from the upper Ellensburg Formation at Craigs Hill (unit Mcg$_e$, age site GD04). Two ages came from Pliocene gravels: one from a sandy matrix between gravels (unit QRcg, age site GD05) and one from a sandy interbed (unit QRcs, age site GD06).

A maximum depositional age (MDA) represents the oldest possible age of the deposit that cannot be explained by a single geologic event. Depending on the geologic context of the sample and the source area, the MDA can be an average age of the youngest population of zircons or the age of the youngest single zircon. Where deposition is more continuous than a single event, such as fluvial deposition of detrital zircons, the youngest single grain is used in our study because of the paucity of young grains (n<5) for Miocene units. We encourage and welcome more robust statistical analyses of our U-Pb results for MDAs of

Pliocene—arguably earliest Pleistocene—units that have larger populations of young zircon grains (n>>5).

INFRARED STIMULATED LUMINESCENCE (IRSL)

Luminescence dating techniques were performed on one sample from unconsolidated material of an alluvial fan surface (unit Qaf3, age site GD07, Data Supplement DS03). Detailed methodology can be found in the Data Supplement (Table DS03).

Sedimentary Provenance and Geochronology of Quaternary Units

Pebble and cobble clast rock types and weathering were recorded to determine provenance and help assess relative deposit ages. Observations from 37 clast count sites are summarized as either polymict for Cascade-sourced material or monomict for locally sourced basalt. These granular data, where combined with observations of field relationships and surface morphologies, are used to infer provenance of sedimentary units and help determine their depositional setting (glacial, nonglacial, or undivided). Note clast count sites CC01–05 reside outside of the map area.

The relative ages of Quaternary units were assessed using clast weathering and surface relationships. The degree of weathering is used as a proxy for age, where thinner weathering rinds represent younger units and thicker rings are older (Porter, 1975). Rind thicknesses of basalt clasts are generally a reliable standard for assessing weathering, although basalt clasts from the Teanaway Formation have more discrete weathering rinds compared to the more diffuse rinds of basalt clasts from the CRBG. Distinguishing these two similar looking basaltic units without geochemistry is tenuous. Surface relationships, including relative elevations and surface morphology, aided estimation of relative ages among different unconsolidated Quaternary deposits.

DESCRIPTION OF MAP UNITS

Holocene to Pliocene Nonglacial Deposits

af **Artificial fill (Holocene)**—Rubble of introduced material; cobbles, pebbles, sand, and boulders; poorly sorted and unconsolidated; used for raising roadbeds, trails, railroads, sports fields, Bowers airfield, and other infrastructure.

ml **Modified land (Holocene)**—Rubble of local material; sand- and boulder-sized local material is redistributed to modify topography and form graded landscapes for industrial, agricultural, and residential zones, including but not limited to gravel pits, areas adjacent to Bowers airfield, and Central Washington University campus.

Qp **Peat (Holocene to Pliocene)**—Peat deposits and ephemeral waterbodies; organic and organic-rich sediment; includes peat, gyttja, muck, silt, and clay; typically in closed depressions; mapped in wetland areas and distinctly flat-bottomed depressions; also mapped on the basis of evaluation of color aerial photos where black to dark gray ephemeral ponds and water bodies were not mapped in the published base map. The thickness of most peat deposits is largely unassessed and unknown. Small peat deposits are scattered throughout the map area, typically within alluvium and related to ponding of stagnant water.

Qls **Landslide deposits (Holocene to Pliocene)**—Clastic aggregate; medium brown, weathering is typically mild; generally loose, jumbled, and poorly consolidated; clay- to boulder-sized clasts; angular to subrounded; unsorted, matrix-supported; unstratified and structureless rubble of sand, silt, clay, cobbles, pebbles, boulders, and diamicton of basalt and sandstone of varied amounts; deposit thicknesses are less than 100 ft and typically less than 50 ft; unit is generally restricted to the uplands of the northern map area along steep canyon walls, along south-facing range front dip slopes composed of basalt of the Sentinel Bluffs Member (unit Mvgs) of the GRB, and near and down slopes composed of the Coleman member of the Ellensburg Formation (unit Mcec); deposits are identified as having crisp landform morphology when viewed using hillshades of bare earth lidar products. A "mass-wasting" overlay is also used to delineate ambiguous deposits with landslide-like characteristics (such as hummocky landforms). These suggest mass movement on unstable slopes where evidence for landslide deposits is inconclusive. The ages, timing, and recurrences of both deposits are uncertain.

Qlso **Old landslide deposits (Pleistocene to Pliocene)**—Clastic aggregate; medium brown to light yellowish brown; poorly consolidated; clay- to boulder-sized clasts; angular to subrounded; unsorted, matrix-supported; unstratified and structureless rubble; deposits are identified as having smoother, muted landform morphology when viewed using hillshades of bare earth lidar. Deposits of unit Qlso are generally geographically larger than unit Qls. Unit Qlso is only exposed on the south-facing range front and commonly overlies the Sentinel Bluffs Member. Notably, the Vantage Member of the Ellensburg Formation is also directly above the Sentinel Bluffs Member. Therefore, it is possible that the old landslide deposits as previously mapped—and maintained in this study—could instead be eroded dip-slope exposures of Vantage sandstone that divide the Sentinel Bluffs Member from the stratigraphically higher but locally absent Wanapum Basalt. Significant site S02 marks an animal burrow containing sedimentary rock fragments that may represent landslide deposits or Vantage sandstone. Limited field evidence supports either conclusion (significant site S02). The age, timing, and recurrence of these deposits is uncertain.

Holocene to Pliocene Alluvial Deposits

Stream channel and stream flood (overbank) deposits and terraces. Surfaces of unit Qoa are elevated above surfaces of unit Qia, and surfaces of unit Qia are elevated above active surfaces of unit Qa. Deposits include pebbles, cobbles, sand, silt, clay, peat, and boulders in varying amounts, and colors range from light tannish gray to medium brown. The deposits are fresh to mildly weathered, not compacted or cemented, and include mostly sand and gravel. The grains are typically well rounded, moderately to well-sorted, basaltic (monomict) to Cascade-sourced (polymict) clast compositions, and their thickness varies. Deposits are as follows:

Qa **Alluvium (Holocene)**—Stream channel deposits on active flood plain; unit is narrowly distributed throughout the lowest elevations of the map area and widely distributed in the Yakima River corridor; depositional environment is on active flood plain; zones of this unit have been heavily modified by agricultural cultivation and have map geometries that reflect such modification, such as sharp angles and abrupt terminations. Precise ages of unit Qa are not constrained. Reference localities clast count sites CC31–33.

Qia **Intermediate-aged alluvium (Holocene to Pleistocene)**—Stream flood (overbank) and old channel deposits near active flood plain; unit is widely distributed in the eastern map area and around the Central Washington University campus; surfaces of unit Qia are elevated relative to surfaces of unit Qa. Unit Qia is sometimes indistinguishable from alluvial fan unit Qaf_1 based on lithology, but tends to be found in closer proximity to unit Qa and at lower elevations than unit Qaf_1. Precise ages of unit Qia are not constrained.

Qoa **Older alluvium (Pleistocene)**—Stream flood (overbank) and older channel deposits and terraces above active flood plain; unit is localized to the south-central map area and is loosely correlated with Vashon-age alpine outwash of the Bullfrog subdrift of the Lakedale Drift (unit Qao_{lb}), where elevations of surfaces of units Qao_{lb} and Qoa are similar, but unit Qoa has paleocurrent indicators that come from the north and east as opposed to from the west for unit Qao_{lb}. Unit also correlates with portions of the alluvial fan unit Qaf_2, which also has surfaces of similar elevations, and may be the same unit in some areas. Distinction between units Qoa and Qaf_2 is difficult far from the range front sources of unit Qaf_2 along lower Currier Creek, east of Reecer Creek Road, and west and below unit QRcg. Precise ages of unit Qoa are not constrained.

Qaf **Alluvial fan deposits (Holocene to Pleistocene)**—Alluvial fan and unconsolidated to poorly consolidated debris flows, undivided sand and gravel; colors range from various shades of brown to brownish medium gray; weathering rinds vary from less than 1 mm up to 1 cm; not compacted; silt- to boulder-sized clasts; angular to subrounded; unsorted; clast composition depends on the composition of bedrock from which the unit is derived but is generally basalt; unit thickness varies with age, where older units are generally thicker; Quaternary fan surfaces to the north of the Dry Creek fault of Bentley (1977) are generally locally derived from the GRB, suggesting a different provenance than alpine glacial outwash farther west and south that is sourced from the Cascade Range. These fan-like deposits are likely alluvial in origin because evidence of glacial ice is ambiguous in the northern portions of the map area east of Reecer Canyon.

Unit is further divided and numbered from 1 (lowest and youngest) to 4 (highest and oldest) based on relative elevation above the modern stream level and differences in surface morphologies, where older surfaces are smoother and more deeply incised compared to rougher, younger surfaces with lesser degrees of fluvial incision. Weathering rinds are <1 mm on unit Qaf_1, about 1 mm on unit Qaf_2 and Qaf_3, and >1 mm on unit Qaf_4. Loess is absent on younger surfaces and common on older surfaces. Notably, escarpments related to the Dead Coyote fault are common and crisp within unit Qaf_3, unclear on unit Qaf_2, and absent on unit Qaf_1. The Dead Coyote fault does not cross unit Qaf_4. Indications of glacial outwash are unclear in fans. Age relationships are relative and precise ages for the units are not fully constrained. Infrared stimulated luminescence (IRSL) returns an age of 468.9 ±54.5 ka (age site GD07) for unit Qaf_3 (Data Supplement Table DS03). Reference localities for unit Qaf_3 are clast count sites CC07/GD07 and CC10–12.

QRcg **Oldest alluvium, gravelly unit (Pleistocene to Pliocene)**—Basaltic gravels; yellowish light brown to dark brown, moderately to strongly weathered with weathering rinds greater than 1 mm and up to a few cm thick; moderately compacted; cobbles and pebbles; well-rounded to rounded; moderately to well-sorted, clast-supported; imbrications of clasts suggest southward and westward paleocurrent directions; monomict, basalt dominant and primarily composed of GRB; unit thickness is variable, where south of Dead Coyote fault, unit is on the order of hundreds of feet thick whereas north of the Dead Coyote fault, unit is as thin as 2 ft and may be a thin veneer of sand and gravel directly overlying basaltic bedrock. Unit is common in the eastern and central zones of the map area in Kittitas Valley, where a large area of unit QRcg has steep, west-facing slopes and gentle, east-facing slopes. Unit is sourced from Naneum Canyon and possibly from Wilson Creek to the north. Unit is highly elevated above other alluvial fan and glacial outwash deposits, and thinly drapes over GRB bedrock. Loess is extremely pervasive on these surfaces and silicic caliche is common. Shallow, poorly confined to unconfined groundwater can be found above, between, and below these horizons (Owens, 1995). Escarpments of the Dead Coyote fault are common yet subtly visible within this

unit, and cross an unpublished paleoseismic trench location, the "Dead Coyote trench" of Sherrod and Barnett (significant site S01; B. Sherrod, USGS, oral commun., 2019). The unit contains at least two surfaces of slightly different elevations, where the paleoseismic trench site lies on an alluvial surface delineated by a geomorphic feature line (see brown, dashed lines on map plate) that is 6–12 ft lower than the adjacent surfaces on either side to the east and west. Unit was previously mapped as the side stream facies of Thorp Gravel by Waitt (1979), and previously referred to as "Naneum Gravel" in field trip guides for the Kittitas Valley by Bentley (1977). Unit is contemporaneous with to younger than Thorp Gravel and it is unclear if these two units have similar origins as glacial outwash because evidence of alpine ice is ambiguous in the northern portions of the map area. Notably, exposures of this gravel unit on Craigs Hill exhibit paleocurrents that indicate a source to the north. U-Pb analysis of detrital zircons from coarse-grained basaltic sand between gravels yields an MDA of ≤2.33 ±0.54 Ma (age site GD05, Data Supplement Table DS02). Reference localities at clast count sites CC03, CC04, CC13–15/GD05, CC16, CC18–23, CC30, CC37, and the north end of Craigs Hill south of the John Wayne Trail.

QRcs **Oldest alluvium, sandy unit (Pleistocene to Pliocene)**—Sandy lenses between gravelly unit; light gray to yellowish medium brown, moderately weathered; well-compacted, moderately indurated; fine- to coarse-grained sand (0.1–1.0 mm); subangular to subrounded; poorly to moderately sorted, matrix-supported; containing planar, parallel laminations with bedding and foresets; paleocurrent indicators suggest a different source direction than the western-sourced glaciofluvial outwash of Thorp Gravel (unit Rcgt); the sandy unit is generally composed of varying amounts of quartz, basalt fragments, and plagioclase crystals, where some outcrops have a pumiceous matrix of re-worked tephra (age site GD06); petrographic analysis of fine sand near clast count site CC23 indicates quartzite, plutonic, and metamorphic fragments, which suggests a northern source for material. Unit thickness is less than 30 ft. Unit is irregularly distributed and interfingering throughout unit QRcg. The depositional environment is inferred to be terrestrial fluvial or alluvial, or possibly glaciofluvial. Unit possibly correlates with the upper portion of the Thorp Gravel (unit Rcgt) but unit may also correlate with the Pliocene Ringold Formation in the Pasco Basin (L. Staisch, USGS, written commun., 2020); U-Pb analysis of detrital zircons from a pumiceous sandstone lense yields an MDA of ≤2.06 ±0.84 Ma (age site GD06, Data Supplement Table DS02). Reference locality at age site GD06.

Holocene to Pliocene Glacial Deposits

Morphology and provenance identify distal alpine outwash from the Cascade Range that entered the map area from the west and north. Elevation profiles exhibit (1) progressive eastward flattening of topographic surface dips, and (2) progressive eastward and southward lowering of surface elevations.

With respect to provenance, clast compositions are more commonly polymict in the Yakima River corridor and within the central map area south of Dry Creek fault. Polymict clast compositions include: basalts of Teanaway and CRBG, andesite, conglomerate, sandstone, quartz, red chert, and rare metamorphic rocks. These compositions suggest a Cascade Range source of detritus with possible input from local and northern sources.

Outside of the Yakima River corridor and central map area, glacial outwash deposits channeled through Green Canyon are abundant in basaltic clasts (clast count sites CC01, CC02, CC08, and CC09) and so are less commonly polymict. These deposits represent side stream outwash trains from an alpine glacier(s?) along First Creek. The side stream outwash trains redirected locally sourced basalt of the Teanaway Formation and GRB detritus out of Green Canyon, which lies north of the Yakima River corridor. A transition in depositional environment and clast composition is marked by the southern bend of Cross Section A–A′, where polymict glacial outwash in the west changes to monomict alluvial fans in the east that lack clear glacial origins.

In the east-central portion of the Swauk Prairie 7.5-minute quadrangle left adjacent to the map area, a north-facing hanging valley resides in upper Green Canyon, where First Creek later incised through Green Canyon (L. Wetherell, CWU, oral commun., 2019). As a result, Green Canyon was abandoned as a side stream outwash corridor that routed detritus southward into Kittitas Valley and the western map area.

The southern bend of Cross Section A–A′ roughly marks a west–east transition from polymict glacial outwash in the west to monomict alluvial fans in the east that lack clear glacial origins.

Qaolb **Bullfrog Vashon alpine outwash of the Lakedale Drift (Pleistocene–Holocene?)**—Polymict pebbly sand to pebble gravel; assorted colors including greenish medium gray, light gray, light brown, yellowish medium brown; mildly weathered with weathering rinds less than 1 mm (clast count site CC28); poorly indurated, not cemented; fine to medium sand with common pebbles; subangular to subrounded, equant to oblate; moderately sorted, clast-supported; where not structureless, imbricated clasts generally show a south–southwest paleocurrent direction; thickness is approximately 10–20 ft near Dry Creek and less than 30 ft near Yakima River; unit is found mostly above the floors of the Yakima River and Dry Creek outwash corridors, whereas rare, thin, short, north–south strands of deposits are possibly associated with the Green Canyon corridor; glaciofluvial terrestrial depositional environment is inferred; unit is slightly younger and lower elevation than most of unit Qaf2, roughly at equal elevations with unit Qoa, and is the lowest lying of the glacial outwash units; unit is identified with the Fraser Glaciation of the Puget Lowland and with the late Wisconsin Glaciation of the North American mid-continent (Waitt, 1979); age of Lakedale Drift is approximately 0.01–0.02 Ma (Waitt, 1979); reference locality clast count site CC28.

Qapok **Pre-Vashon alpine outwash of Kittitas Drift, undivided (Pleistocene)**—Sand and gravel, where basalt weathering rinds are on average about 1 mm thick. Unit includes Indian John and Swauk Prairie subdrifts, which are divided primarily on differences in terrace elevation because weathering rind thicknesses and provenances are nearly identical. Provenance includes polymict and monomict varieties. Outside of the Yakima River corridor, these deposits were sourced from Green Canyon to the north, which has a variety of rock types at higher latitudes and elevations and gets progressively monomict at lower latitudes and elevations toward the mouth of Green Canyon. We speculate that the change in composition of outwash trains may be recording outwash channel reorganization related to recession of alpine ice away from polymict clast sources and toward monomict ones. These provenance changes may also reflect other outwash trains utilizing other outwash corridors over and through Horse Canyon and Dry Creek to the west for polymict varieties. Ellensburg Blue agates can be found scattered on the subunits of Kittitas Drift south of Green Canyon. Landowners report finding petrified wood (fossilized palm trees?) in hay fields near the Number 9 Hay processing facility, west of clast count site CC30, on mapped outwash surfaces. Age of Kittitas Drift is inferred to be approximately 0.13–0.14 Ma (Waitt, 1979). Kittitas Drift is subdivided into:

Qapoki **Indian John pre-Vashon alpine outwash (Pleistocene)**—Polymict to monomict cobble and pebble gravel with greater proportions of cobbles than pebbles; medium to dark brown exposures with clasts of assorted colors, including medium brown, yellowish light brown, greenish medium gray, light to dark gray, deep red, white, and moderately weathered with basalt clasts having weathering rinds approximately 1 mm thick; poorly cemented, semi-consolidated; subrounded to well-rounded where clast shapes are more commonly oblate than equant; poorly sorted, matrix-supported in a sandy matrix; poor exposures are structureless; clast compositions in order of decreasing abundance are: basalt, andesite, conglomerate, sandstone, white quartz, red chert, and metamorphic rocks. Basaltic clasts generally have sharp weathering rinds, suggesting basalt of the Teanaway Formation compositions rather than CRBG rocks that have diffuse weathering rinds (Porter, 1975). Unit thickness can be up to 50 ft. Unit is found mostly in the western half of the map area north of Yakima River and south of Green Canyon, or south of Yakima River. A glaciofluvial terrestrial depositional environment is inferred. Loess is less pervasive on these surfaces. Unit approximately correlates with older portions of alluvial fan unit Qaf_2. Reference locality clast count site CC29.

Qapoks **Swauk Prairie pre-Vashon alpine outwash (Pleistocene)**—Polymict to monomict sandy, cobble-to-pebble gravel; light to medium brown, moderately to strongly weathered with basalts having weathering rinds 0.5–1.0 mm and as large as 2.5 mm on larger cobbles; poorly to mildly cemented, semi-consolidated; subrounded where clast shapes are more commonly oblate than equant; poorly sorted, clast-supported; sandy interbeds 3–4 ft thick between gravels, and clast imbrication indicates southward paleocurrent direction; thickness can be up to 50 ft; exposures are common on the western half of the map area north of Yakima River and south of Green Canyon, or south of Yakima River; glaciofluvial terrestrial depositional environment is inferred; loess is common on these surfaces; hard impermeable silicic caliche is commonly developed within 2 ft below ground surface, and shallow unconfined to poorly confined groundwater can be found above, between, and below these horizons (Owens, 1995); unit approximately correlates with alluvial fan unit Qaf_3 and younger portions of unit Qaf_4; reference locality clast count sites CC01, CC08, and CC09.

Rcgt **Thorp Gravel (Pliocene)**—Glacio(?)-fluvial gravels with sand; medium brown exposures of multicolored clasts including light to dark brown, light to dark gray, white, orange, greenish gray, maroon to red; strongly weathered with basalt clasts having weathering rinds ranging from 1–20 mm but commonly 2–5 mm wide; moderately to well-cemented, moderately indurated; cobbles and pebbles with fine- to coarse-grained sand; rounded with oblate to equant shapes; moderately to well-sorted, clast-supported; clasts are polymict with andesite, basalt, conglomerate, sandstone, vein quartz, chalcedony, chert, intrusive rock, and metamorphic rock. Sandy matrix is light brown to tan; poorly to mildly consolidated; moderately cemented; subangular to subrounded; moderately to well-sorted; sand composition contains proportions of quartz greater than feldspar greater than or equal to lithic fragments (Q>F≥L). Imbricated gravel clasts suggest southward and eastward paleocurrent directions. Unit thickness ranges from hundreds of feet (<300 ft) in the western map area to tens of feet (20–50 ft) in the central map area. Previously mapped as the mainstream facies of

Thorp Gravel by Waitt (1979). Moraines mapped by Porter (1976) west of the map area suggest that the Thorp Gravel may be glaciofluvial outwash, terrestrial, and sourced from the Cascade Range, whereas an alternative origin for the unit is proposed by Waitt (1979), who argued that unit represents aggradation caused by local tectonic activity. Capping loess is pervasive (<3 ft thick) and silicic caliche is common (at least 1 cm thick). Shallow, poorly confined to unconfined groundwater can be found above, between, and below these horizons (Owens, 1995). Tephras interbedded in gravels on the south-facing exposures of the highest terrace north of the Yakima River and west of the map area yielded fission track ages of 3.64 ±0.74 Ma and 3.70 ±0.20 Ma (Waitt, 1979). Unit may correlate with the Pliocene Ringold Formation in the Pasco Basin. Reference localities are clast count sites CC17 and CC24.

Tertiary Sedimentary and Volcanic Bedrock

SEDIMENTARY ROCKS OF THE ELLENSBURG FORMATION

Mce **Ellensburg Formation, undivided (Miocene)**—Volcaniclastic to lacustrine or fluvial sedimentary bedrock underlying, intercalated with, and overlying rocks of the CRBG; light to medium brown to light to medium gray; mildly weathered; moderately to well-indurated; exposures can vary from thin, discontinuous, poorly exposed interbeds in GRB with lighter color tones on aerial imagery to well-exposed contiguous outcrops along cliffs, topographic saddles, and ditches; as intercalated interbeds in GRB, unit can be commonly identified where vegetation preferentially grows from sedimentary soils with higher permeability rather than basalt; thickness is generally less than 300 ft; unit Mce is generally mapped where outcrops are absent; where outcrops are available, unit is divided based on grain size into:

Mcfe **Siltstone (Miocene)**—Pumiceous, diatomaceous(?) siltstone or possibly re-worked, non-welded tephra; light gray to yellowish white, fresh to mildly weathered; lightweight, low density, moderately indurated to friable, mildly cemented; silt to fine-grained sand (0.05–0.1 mm, as large as 0.25 mm); subangular; well- to moderately sorted; common planar, parallel laminations; sand composition is ashy and pumiceous with highly variable composition of feldspar (ranging from 10–50%, but typically between 10–25%), including alkali feldspar and possibly plagioclase feldspar, without quartz, and containing trace mica (<1%, <0.3 mm); within the resolution limits of our microscope, biogenic siliceous skeletons are not obvious and may not be present; unit thickness is generally less than 200 ft; unit is located in the northern map area, interbedded between GRB members of Sentinel Bluffs and Grouse Creek; a lacustrine or fluvial depositional environment is inferred (Smith, 1988a,b); contacts pinch out over short distances; age is Miocene, where U-Pb analyses of detrital zircons yield an MDA ≤14.87 ±1.32 Ma (age site GD01) and ≤15.77 ±1.14 Ma (age site GD03) (Data Supplement Table DS02). Detrital zircon provenances from these sites may be similar to the Ringold Formation (L. Staisch, USGS, written commun., 2020) suggesting a long-lived fluvial system deposited far-sourced sediment into an area north of Kittitas Valley. Reference localities are sites GD01, GD03, and G18.

Mcse **Sandstone (Miocene)**—Micaceous feldspathic sandstone; yellowish light to medium brown; poorly indurated, poorly cemented; coarse- to fine-grained sand; subrounded; well sorted; structureless(?); sand composition includes feldspar and lithic fragments of basalt with rare white mica; unit thickness is less than 100 ft; a fluvial or lacustrine depositional environment is inferred (Smith, 1988a,b); interbedded in the Sentinel Bluffs Member and pinches out over short distances; unit is less pervasive than siltstone unit Mcfe; reference locality north of age site GD03.

Mcge **Gravelly unit (Miocene)**—Polymict, laharic conglomerate with lenses of sandstone and non-welded ash with minimal to no sedimentary re-working; yellowish medium to light brown to light-to-medium brownish gray, sometimes orange-brown, moderate to strong weathering; moderately cemented, poorly to moderately indurated; cobble to pebble gravel (0.5–9.0 cm) with boulders in a matrix of fine- to very coarse grained sand (0.2–2.0 mm); clasts are subrounded with oblate to equant shapes, grains in matrix are generally subrounded with few being rounded and even fewer being subangular; poorly sorted, clast-supported; structureless to bedded gravels with accretion sets (foresets and truncation surfaces) of sandstone lenses with rare cross-bedded sands; gravels are polymict with assorted clasts including basalt, andesite, rhyolite, sandstone, quartz, tuff, pumice, granite, and rare metamorphic

rocks(?); sand composition is variably pumiceous (15–30%, 1–5 mm) with quantities of other clasts being as follows: plagioclase greater than hornblende greater than pumice greater than or equal to glass (5–10%, 0.35–0.5 mm, black, angular, sharp) greater than or equal to lithic fragments of quartzite, basalt, andesite, pumice, carbonate(?), metamorphic rock(?), and rare mica; thickness is greater than 100 ft; exposed on west-facing slopes of Craigs Hill in the southern map area and along State Route 10, west of Eagles Rest Road, north of the Yakima River off the map area to the west; depositional environment is inferred to be terrestrial, fluvial, and possibly the distal extent of a lahar (Smith, 1988a,b); white clastic dikes are present on Craigs Hill exposure (as large as 6–12 in. wide) (Mabry, 2000); lower contact is not observed, and upper contacts with the Thorp Gravel (unit Rcg$_t$) and "Naneum Gravels" (unit QRcg) are angular unconformities with the younger units incising and producing erosional surfaces in unit Mcg$_e$; an $^{40}Ar/^{39}Ar$ age from a laminated interbedded tephra on the north side of Craigs Hill yields an age of 4.90 ±0.10 Ma (age site GD08) (figure 3 of Lamb, 1997). Reference localities are at the north end of Craigs Hill and clast count sites CC34–36.

Mc$_{ec}$ **Coleman member of the Ellensburg Formation, undivided (Miocene)**—Sandstone and siltstone underlying the Sentinel Bluffs Member and directly overlying the Grouse Creek member. Informally named by Bentley (1977) near Coleman Canyon of northern Kittitas Valley and mapped by Hammond (2013) as far south as the Naches River area. It is equivalent to the eponymous Rock Island member of Hoyt (1961) farther north, the Douglas Creek member of Ebinghaus and others (2015), and Rock Island arkosic sands of Schmincke (1967). Less than 300 ft thick of well-exposed sedimentary outcrop. Divided into subunits by grain size, and can contain basaltic boulder-sized exposures of Winter Water and Wapshilla Ridge Members (geochemistry sites G25 and G29, respectively) that may be in-place basalt outrcrops. Good exposures can be found in roadside ditches of Wilson Creek Road on Lillard Hill in the eastern map area and along cliffs on Hart Road on the west flank of Lookout Mountain off the map area to the west. Landslides commonly form downslope of exposures. The Coleman member may form a prolific aquifer at depth in the Kittitas Valley. The Coleman member is divided into:

Mcf$_{ec}$ **Siltstone (Miocene)**—Pumiceous, diatomaceous(?), micaceous siltstone; white to yellowish white, mildly weathered; light weight, low density, mildly to moderately indurated, mildly cemented and can be friable; fine-grained sand (0.1–0.2 mm); subangular; moderately sorted; planar, parallel laminations upon which micas preferentially settle; sand composition contains mica (2–4%, 0.2–0.3 mm) and quartz- and mica-rich lithic fragments (in lithic fragment, micas are <20%, 0.4–0.7 mm, biotite>muscovite); thickness is less than 200 ft; located in topographic saddles behind faceted spurs of the range front in the northern map area; depositional environment is inferred to be lacustrine or possibly fluvial (Smith, 1988a,b); underlies the basalt of McCoy Canyon of the Sentinel Bluffs Member and directly overlies the Grouse Creek member; age is inferred to be Miocene; reference locality geochemistry site G29.

Mcs$_{ec}$ **Sandstone (Miocene)**—Micaceous feldspathic sandstone; white to light gray with hues of yellow, orange, and light blue, mildly weathered to fresh; poorly to moderately cemented, moderately indurated, well-consolidated; generally medium-grained sand (0.15–0.3 mm), but can range from fine- to coarse-grained sand; relative proportions of subangular grains are greater than or equal to subrounded grains; well-sorted; structureless to laminated with planar, parallel laminations; sparse, planar, dark brown resistant layers (<1.5 cm thick, iron or magnesium oxides?), may include conjugate joint sets with orientations ranging from north-northwest- through north-northeast-striking and steeply dipping >70°; sand composition includes quartz greater than feldspar greater than

lithic fragments (Q>F>L); lithic fragment content contains variable amounts of basalt fragments from absent (age site GD02) to abundant (geochemistry site G25), includes trace quartzite, and is variably micaceous (generally 3–10%, <0.5 mm, and ranging 1–17%, 0.2–2.0 mm) with biotite (weathered copper brown and black to a lesser degree) and muscovite (mostly clear, some light brown), does not react when 10 percent hydrochloric acid is applied; thickness is less than 200 ft; located in topographic saddles behind faceted spurs of the range front in the northern map area; depositional environment is inferred to be fluvial or lacustrine (Smith, 1988a,b); underlies the basalt of McCoy Canyon of the Sentinel Bluffs Member or the Ortley member and directly overlies the Grouse Creek member; new U-Pb analysis of detrital zircons yields an MDA ≤46.76 ±2.72 Ma (age site GD02, Data Supplement Table DS02; sample is devoid of Miocene zircons), but age is inferred to be Miocene despite an Eocene MDA because: (1) unit is between members of Miocene GRB; and (2) pumiceous siltstones, sampled below (GD01) and above (GD03) the horizon, indicate a ~16 Ma MDA; unit may also correlate with the Slack Canyon sandstone that underlies the Winter Water Member in three areas: near the Saddle Mountains, in the Columbia Gorge near Hood River, and near the White Salmon River and Sentinel Bluffs (S. Reidel, WSU Tri-Cities, oral commun., 2020); reference locality sites GD02 and G25.

VOLCANIC ROCKS OF THE COLUMBIA RIVER BASALT GROUP

Basaltic andesite; very dark gray to medium gray where fresh, medium to dark brown where weathered, typically mildly weathered to fresh; dense and hard; aphyric, generally aphanitic, where crystals in the groundmass can vary from ~0.1 mm to a few millimeters; commonly with flows exhibiting the following physical characteristics: basal, columnar-jointed colonnades, interior entablatures, and capping vesicular flow tops; many volcanic units of the CRBG are comprised of multiple lava flows, and contacts between lava flows of the same unit are separated by solid or dashed, gray lines on the map; terrestrial lava flows of the CRBG are locally divided into the following units, where flows are named following Reidel and Tolan (2013):

Mvw **Wanapum Basalt, undivided (Miocene)(cross section only)**—Basalt. Subsurface existence of Wanapum Basalt is inferred based on the well log interpretations of Jones and others (2006), Jones and Vaccaro (2008), Vaccaro and others (2009), and on interpretation of gravity and magnetic anomalies. The northernmost extent of Wanapum Basalt in the subsurface of the map area is unclear and inferred to be south of the Dead Coyote fault because Wanapum-type compositions were not observed from samples analyzed for whole rock geochemistry.

Mvg **Grande Ronde Basalt (GRB), undivided (Miocene)**—Basaltic andesite described in detail in the following units. GRB members are broadly mappable using a portable fluxgate magnetometer to place units into a magnetostratigraphic context. Previously mapped according to four polarity-chronostratigraphic units or magnetostratigraphic units (MSU). From oldest to youngest: reverse magnetic polarity 1 (R1 MSU), normal magnetic polarity 1 (N1 MSU), reverse magnetic polarity 2 (R2 MSU), and normal magnetic polarity 2 (N2 MSU) (Tabor and others, 1982; Reidel and Tolan, 2013; Hammond, 2013). Unit Mvg is mapped where geochemistry was unavailable, outcrops were lacking, inference for a subunit was overly speculative, or units were grouped at depth in cross section (for example, R1 and N1 MSU or Ortley and Winter Water members).

Stratigraphy in our map area is remarkably similar to the stratigraphy of Hammond (2013) in the Naches River area. Without the base exposed, total thickness of GRB rocks is poorly constrained. The thickness is inferred from geophysical modeling of gravity and aeromagnetic data, and may range from approximately 2,500–3,800 ft thick north of Dead Coyote fault. Models of the geophysical data show thinner GRB in the range front and thicker in the middle of Kittitas Valley. CRBG thickness is interpreted from two hydrocarbon exploration boreholes ~12 mi east and southeast from the map area: Shell BISSA 1-29 well (API# 046-037-00006) and Meridian BN 23-35 well (API# 046-037-00009). These suggest thicknesses of ~4,600 ft and ~6,700 ft, respectively (Wilson and others, 2008; Czajkowski and others, 2012), but do little to tightly constrain GRB thickness within the map area. With geophysical data modeling proposing thicker CRBG in the middle of Kittitas Valley, and these wells, particularly BN 23-35, being closer to the synclinal axis of the valley, we would expect available well data to show thicker CRBG overall. The northern map area is composed primarily of GRB with sedimentary interbeds. In general, thin sections show more euhedral than subhedral laths of plagioclase microlites intermeshed in an irregular, unoriented groundmass texture (felty to pilotaxitic

more than trachytic) with incomplete details of mafic mineral compositions and percentages.

Where whole rock geochemistry was available, a Machine Learning (ML) model developed at the Washington State University (WSU) GeoAnalytical Laboratory classified samples into established CRBG stratigraphy (see *Whole Rock Geochemistry Results*). As such, GRB is divided into:

Mvgs **Sentinel Bluffs Member, undivided (Miocene)**—Basaltic andesite; aphyric, aphanitic; the map area contains four subunits, from oldest to youngest: basalts of McCoy Canyon, Stember Creek, Spokane Falls, and Museum, where the middle two subunits are portions of the "Cohassett flow" (Reidel, 2005) that may be intermingling compositional types and may locally exhibit an internal vesicular zone (IVZ) related to "flow inflation" between the basalts of Spokane Falls and Stember Creek (McMillan and others, 1989; Reidel, 2005). If present locally, the IVZ may obscure the locations of vesicular flow tops identified via surface mapping of physical volcanology characteristics, whereby vesicular flow tops may look like the IVZ and vice versa. The Sentinel Bluffs Member is at least ~600 ft thick. The unit is thinnest on Dead Coyote anticline, possibly as a result of uplift and erosion, and is likely thicker in synclines and in Kittitas basin. The Sentinel Bluffs Member is commonly located along the northern margins of Kittitas Valley or higher elevations near Table Mountain in the northern map area. The unit was formerly mapped as GRB N2 MSU (Tabor and others, 1982). Unit Mvgs is mapped where geochemistry was unavailable, but reasonable interpolations could be made using existing geochemical results (generally TiO_2<2.0 wt. %, MgO>3.8 wt. %); with available whole rock geochemistry, the Sentinel Bluffs Member is subdivided into:

Mvgsm **Basalt of Museum (Miocene)**—Basaltic andesite; aphyric, aphanitic to medium crystals (<0.6 mm); mostly entablature with rare basal colonnade at two geochemistry sites (G06 and G47); TiO_2: ~1.72–1.87 weight percent, MgO: ~3.8–4.8 weight percent, P_2O_5: ~0.30–0.35 weight percent; whole rock geochemistry samples are all confidently classified as Museum 1 of Hammond (2013) except for the site G12 sample, which is a compositional outlier and may be the younger Museum 2 composition of Hammond (2013); geochemical fields of Museum 2 and Meeks Table flow (Hammond, 2013) of Grouse Creek member generally overlap; unit thickness is ~160–250 ft and may be thicker in synclines and in Kittitas basin; contains 3–4 flows; unit is widespread and found along lower portions of northern range front, shallowly underlying pediments (units QRcg through Qaf2) north of the Dead Coyote fault, and at highest elevations toward Table Mountain; upper contacts with Vantage Member or Wanapum Basalt are not exposed in the map area; pahoehoe texture observed at significant site S04; reference localities include geochemistry sites G06/M01, G45–G47, and G49.

Mvgssf **Basalt of Spokane Falls (Miocene)**—Basaltic andesite; aphyric, aphanitic to fine crystals (<<1.0 mm); common basal colonnade, interior entablature, and vesicular flow top; rare microphenocrysts (<1.0 mm) of plagioclase, mafic mineral percentages 15–25 percent; TiO_2: ~1.8–1.9 weight percent, MgO: ~4.3–5.0 weight percent; unit thickness is ~150–300 ft and may be thicker in synclines and in Kittitas basin and, notably, unit thickness in the BISSA well farther east is ~640 ft (S. Reidel, WSU Tri-Cities, written commun., 2020); contains 1–3 flows, thin hyaloclastite horizons, and interfingers with Stember Creek-type compositions (geochemistry sites G39 and G40, possibly near IVZ); found commonly in northern range front and higher elevations toward Table Mountain; upper and lower contacts generally inferred using changes in physical volcanology paired with geochemical results. Reference localities include geochemistry sites G04, G05, G10, and G24.

Mvgssc **Basalt of Stember Creek (Miocene)**—Basaltic andesite; aphyric, aphanitic to medium crystals (~0.3 mm); common basal

colonnade, interior entablature, and vesicular flow top; mafic mineral percentages 25–38 percent; TiO_2: ~1.72–1.82 weight percent, MgO: ~4.8–5.05 weight percent, P_2O_5: ~0.25–0.30 weight percent, unit thickness is less than ~150 ft and may be thicker in synclines and in Kittitas basin; contains at least one flow, possibly pinches out northward and interfingers with Spokane Falls-type compositions (geochemistry sites G39 and G40, possibly near IVZ); unit is not commonly identified in the map area and is less common than the basalt of Spokane Falls; reference locality includes geochemistry site G31.

Mvgsmc **Basalt of McCoy Canyon (Miocene)**—Basaltic andesite; aphyric, aphanitic to fine crystals (~0.2 mm); forms good entablature with short basal colonnade and common vesicular flow top; rare large (<1.0 mm) microphenocrysts of plagioclase, mafic mineral percentages 20–30 percent; geochemistry samples G23, G32, and G33 (TiO_2: ~1.91–1.96 wt. %, MgO: ~4.59–4.73 wt. %, P_2O_5: ~0.27–0.30 wt. %) are confidently classified as Lower McCoy Canyon of Hammond (2013), whereas geochemistry sample G51 (TiO_2: ~1.83 wt. %, MgO: ~4.8 wt. %, P_2O_5: ~0.32 wt. %) is confidently classified as Upper McCoy Canyon of Hammond (2013); unit thickness is ~150–200 ft and may be thicker in synclines and in Kittitas basin; contains at least one or two flows, possibly pinching out northward; forms outstanding faceted spurs on the range front of unit Mvgssf and commonly overlies the Coleman member of the Ellensburg Formation; reference localities include geochemistry sites G32 and G51.

Mvgw **Winter Water Member (Miocene)(cross section only)**—Basaltic andesite; light to dark brown, moderately to strongly weathered; unit thickness is less than ~100-ft, may be thicker in synclines and in Kittitas basin; pinches out locally; may represent an erosional surface onto which the Coleman member deposited; reference locality only includes geochemistry site G25 within unit Mcsec.

Mvgo **Ortley member**—Basaltic andesite; aphyric, aphanitic to fine-grained; contains well-developed fanning or platy entablature; unit thickness is ~100-ft thick, may be thicker in synclines and in Kittitas basin; pinches out locally; includes at least one flow; may represent an erosional surface onto which the Coleman member deposited given their close proximity; reference localities include geochemistry sites G02 and G09.

Mvgg **Grouse Creek member (Miocene)**—Basaltic andesite; aphyric, aphanitic to medium crystals (<0.8 mm); commonly features hyaloclastite (and (or) peperite?); very dark gray to dark brownish gray, mildly to moderately weathered, and slightly more weathered than other GRB; groundmass crystal sizes are slightly greater than units of Mvgs; TiO_2: 1.8–2.1 weight percent, MgO: 3.7–4.3 weight percent, P_2O_5: ~0.27–0.35 weight percent; mostly fanning entablatures, rarely platy (geochemistry site G07), where colonnades and vesicular tops are thin, poorly developed to absent in the unit's interior; mafic mineral percentage 10–35 percent (0.2–0.5 mm) depending on the flow; WSU's ML model returned low confidence classifications for nearly all samples of the unit. Local stratigraphic relationships place the unit above the Wapshilla Ridge Member and below the Basalt of McCoy Canyon. Geochemical results plot in the field for the Meeks Table flow on TiO_2 vs. MgO and TiO_2 vs. P_2O_5 diagrams using data compiled from Hammond (2013). Note, geochemical fields of Meeks Table flow (Hammond, 2013) of Grouse Creek member and Museum 2 generally overlap. Geochemical data from Hammond (2013) was not included in the geochemical training set for the ML model. Therefore, insufficient training of the ML model may be responsible for the low confidence classifications of unit Mvgg geochemistry results. Unit thickness is ~700–1,000 ft and may be thicker. Breaks in fanning entablatures show at least two flows and probably more (less than six). Unit spans mid-elevations in the northern map area. Unit is commonly associated with hyaloclastite, especially where directly underlying the Coleman member, and likely

contains portions that are invasive. Previously mapped as the Howard Creek invasive flow by Rosenmeier (1968) and (or) GRB R2 MSU by Tabor and others (1982). Lower contact with Wapshilla Ridge Member is inferred according to a topographic bench interpreted to be a flow break of resistant vesicular top of unit Mvgwr. Unit is exposed in a monocline with minor faulting. Significant site S03 exhibits pahoehoe texture. Reference localities include geochemistry sites G03, G13, G15, G16, and G35.

Mvgwr **Wapshilla Ridge Member (Miocene)**—Basaltic andesite; aphyric, aphanitic to medium crystals (<1.0 mm); contains well-developed basal colonnades and vesicular tops and common entablatures; microphenocrysts of plagioclase (typically 0.05–0.15 mm and can be as large as 0.8 mm), clinopyroxene (<10%, <0.8 mm), and olivine (<5%, 0.3–0.5 mm, mildly altered to iddingsite) in a felty groundmass of plagioclase microlites; TiO_2>2.1 weight percent, MgO>3.2 weight percent; unit thickness is at least ~300 ft and is likely thicker (<1,000 ft?); contains at least one or two exposed flows; best exposed in Wilson Creek, base is not exposed; reference localities include geochemistry sites G01 and G034.

PRE-MIOCENE BEDROCK

Ec **Continental Sedimentary Rocks, undivided (Oligocene to Eocene)(cross section only)**—Unit may include tuffaceous siltstone and sandstone of the Oligocene to Eocene Ohanapecosh Formation; coaliferous sandstone, tuffaceous(?) siltstone, and minor rhyolite of the Eocene Roslyn Formation; and (or) sandstone and conglomerate of the Eocene Swauk Formation. Unit is interpreted as entirely Eocene in age beneath unit Evt.

Evt **Teanaway Formation, undivided (Eocene)(cross section only)**—Primarily basalt with tuff and may include dikes, related intrusions, volcaniclastic rocks, and rhyolite(?).

LITHOLOGIES DEPICTED AS OVERLAYS

Quaternary loess and Miocene hyaloclastite were mapped as overlays in the map area. Quaternary loess was mapped as an overlay so as not to obscure the contact relationships among the glacial and alluvial units that it blankets. This way the contact relationships between those older Quaternary units are emphasized. Miocene hyaloclastite was mapped as an overlay because we wanted to show the lithology's extent and how its abundance decreases to the west. In the case of the hyaloclastite, this addresses previous mapping by Tabor and others (1982) that shows an irregular contact relationship between invasive and non-invasive reverse polarity GRB (MSU R2) drawn as a straight dashed line east of the map. Our approach clarifies this delineation and more precisely shows where those lavas may have been invasive.

Mass Wasting (overlay mw)

Landforms suggest mass movement on unstable slopes, but evidence for landslide deposits is inconclusive.

Quaternary Loess (overlay Ql)

Eolian loess is described as the following: light brown to medium brown, moderately weathered; low density, poorly compacted; silt to very fine grained sand (less than 0.15 mm); angular; moderate to poor sorting, matrix-supported; internally structureless forming 3-foot-tall, irregularly spaced mounds with varying amounts of post-depositional fluvial dissection; windblown loess is widespread and most commonly blankets older alluvial and glacial outwash (units QRcg, Rcgt, Qapoks, Qaf3) in the central to northern map area. Deposits are found on flat to gently sloping surfaces where they cover units of various ages and elevations, and preferentially on the east-facing and leeward slopes where deposits are sheltered from modern prevailing winds. Locally, loess mounds are also called patterned ground or Manastash Mounds, and are not to be confused with Mima mounds of western Washington. Loess mounds are likely the result of intensive frost action under a periglacial climate (Kaatz, 1959; Williams and Masson, 1949); anastomosing surface textures with ~1–3 ft deep incisions that are ~2–15 ft wide suggest that fluvial incision and erosion may also aid generation or modification of these mound landforms. Loess deposits have been heavily modified by agricultural cultivation and have map geometries that reflect such modification (such as sharp angles and abrupt terminations). This deposit correlates with the eolian loess of the Palouse Formation, found throughout eastern Washington. Two thermoluminescence ages from Craigs Hill loess (Lamb, 1997) estimate the age of the unit locally as young as 24 ±2 ka to as old as 29 ±4 ka. Age is roughly Holocene to Late Pleistocene.

Miocene Hyaloclastite (overlay hy)

Hyaloclastite is described as the following: a volcaniclastic aggregate, pillow breccia, and peperite(?); light yellowish brown to orange brown or tan, strongly weathered; moderate density, moderately well consolidated; generally sand to boulder grain size with a very fine grained matrix (less than 0.05 mm); angular to subangular; poorly sorted, matrix-supported; generally convoluted and structureless, and exposures may contain basalt pillows; centimeter- to meter-scale pillow fragments can have centimeter-scale columnar-jointed corrugations on their surfaces; clastic aggregates characteristically include obsidian, palagonite, and plagioclase crystal fragments; thickness varies from several feet up to about 150 ft; unit is associated with basaltic exposures of the Grouse Creek member (unit Mvgg) and basalt of Spokane Falls (unit Mvgssf) in the northern and central map area. In the case of the Grouse Creek member, exposures of contiguous planar(?) hyaloclastite directly underlie the Coleman member

of the Ellensburg Formation (unit Mcec) and decrease westward toward Green Canyon. These lithologic characteristics and spatial associations suggest that the hyaloclastite was locally generated from quenching with consequent fracturing, disintegration, and weathering of GRB lavas as they entered a Miocene water body. A thin sedimentary interbed at significant site S03 suggests that portions of unit Mvgg with hyaloclastite may be an invasive basalt flow or peperite as previously mapped (Rosenmeier, 1968; Tabor and others, 1982). Age is presumed to be similar to the Miocene basalts they reside in. Reference localities for hyaloclastite include areas south of geochemistry sites G35 and G20, at geochemistry site G48, and at significant site S03.

WHOLE ROCK GEOCHEMISTRY RESULTS

A Machine Learning (ML) model developed by researchers at the Peter Hooper GeoAnalytical laboratory of Washington State University was used to categorize a regional compilation of CRBG rocks with whole rock geochemical analyses. The ML model compared our 49 samples of basaltic rock (Data Supplement Table DS01) to their regional compilation. The ML model compares elemental compositions and returns a confidence rating for how similar our new data are to existing data from CRBG formations and members. All 49 samples matched Grande Ronde Basalt (GRB) chemistries at greater than 99 percent confidence. Our samples are further divided into, from youngest to oldest: Sentinel Bluffs Member (n=26); Winter Water Member (n=1); Ortley member (n=3); Grouse Creek member (n=16); and Wapshilla Ridge Member (n=3). The Sentinel Bluffs Member is further subdivided from youngest to oldest: basalt of Museum (n=9), basalt of Spokane Falls (n=9), basalt of Stember Creek (n=3), and basalt of McCoy Canyon (n=5). Confidence ratings were generally high for most samples (over 80%). Samples with low confidence classification (4–34%, usually <10%) are ambiguously classified by the ML model as four possible members (oldest to youngest): Downey Gulch, China Creek, Grouse Creek, or Ortley. For such samples, we compared our new unnormalized whole rock geochemistry results to unnormalized GRB geochemical results of Hammond (2013) from nearby Naches, WA using two-axis plots of TiO_2 vs. MgO and TiO_2 vs. P_2O_5 (Fig. 1A and 1B, respectively). Compositional fields for the GRB units were hand drawn according to Hammond's data only to assist categorization of low confidence samples from the ML model. These fields were meant to be approximate guidelines and not firm boundaries. We found our results compared similarly to CRBG stratigraphy of Hammond (2013), and our samples with low confidence ratings broadly match geochemically and stratigraphically with Hammond's Meeks Table flow(s) of the Grouse Creek member. Assuming a simple layer-cake model of eruption during the middle Grande Ronde, the Downey Gulch and China Creek compositional types reside much lower in the stratigraphic section compared to Grouse Creek. It is unlikely that these lower confidence samples could be classified as the older members, as this would require complicated eruptive histories or complex structural relationships that were not observed. Additionally, the low confidence samples do not reside in the Ortley compositional type-field (Fig. 1). For all of these reasons, the low confidence samples are inferred to be Grouse Creek-type compositions. As of August 2020, geochemical data from Hammond (2013) is not incorporated into the training dataset for WSU's ML model so ML classifications do not well characterize the middle portion of our stratigraphy. In general, samples with Sentinel Bluffs-type compositions have lower SiO_2 content (~53.7–55.7 wt. %), lower TiO_2 content (<2.0 wt. %) and higher MgO content (~3.8–5.1 wt .%), whereas older GRB units have higher SiO_2 (~54.7–57.7 wt. %), higher TiO_2 (~2.0–2.3 wt. %), and lower MgO (<4.2 wt. % MgO).

Most GRB samples are basaltic andesite (Fig. 2A) (Le Bas and others, 1986). Three GRB samples that aren't basaltic andesite plot in the andesite field on the total alkali silica (TAS) diagram (geochemistry sites G09, G29, G42). These samples may not have representative geochemistries because they are platy interior colonnade (site G09), are surrounded by sandstone (site G29), or are a vesicular flow top (site G42).

From non-normalized geochemical data (n=49), most GRB samples are tholeiitic with eight notable exceptions in the Sentinel Bluffs and Wapshilla Ridge Members (Figure 2B). Seven samples with Sentinel Bluffs-type chemistries exhibit calc-alkaline results (geochemistry sites: Museum = G12, G47, G49. Spokane Falls = G11, G50. Stember Creek = G31. McCoy Canyon = G51) and were found south of the range front and north of a large fault (Dead Coyote fault), where fluid circulation near the fault may have affected the whole rock geochemistry. One sample with Wapshilla Ridge-type chemistry (geochemistry site G29) was also calc-alkaline and may be related to its cropping out within the Coleman member. All ternary results for eight samples reside near the calc-alkaline-tholeiitic boundary.

GEOPHYSICS

Potential-fields geophysics—gravity and magnetics—reveals subsurface zones of variation in density or magnetic properties, respectively. Such variations can help reveal the extent of formations in the subsurface or structures that abruptly change their extents or depths, like faults and folds (Figure M1).

Geophysical Interpretations

In the Kittitas Valley region, gravity and aeromagnetic anomalies (highs, lows, and gradients) are interpreted together in the following ways. Using the contours on Figure M1A, gravity highs represent shallower basement, such as near Table Mountain along the northern edge of the map area. Gravity highs can also represent regions with thicker basalt in the subsurface. Conversely, gravity lows result from deeper basement and thicker near-surface sediments such as the Ellensburg Formation and Quaternary deposits. Magnetic highs correspond with thicker layers of normally magnetized basaltic rock in the subsurface (magenta and red on Figure M1A). Strong magnetic lows originate from basaltic rock with strong reverse remanence or sediment in the shallow subsurface (blue on Figure M1A). Gradients in either potential-fields dataset indicate that geophysical characteristics are changing over a short distance and may be interpreted as faults or folds when compared to available geologic data. Volcanic units with similar magnetic properties cannot be differentiated in our data or modeling. Some areas of the aeromagnetic data (Blakely

and others, 2020a,b) disagree with the magnetostratigraphy of prior GRB mapping (Tabor and others, 1982).

INTERPRETATIONS RELATED TO PRE-MIOCENE ROCKS AND BASIN ARCHITECTURE

High gravity near the northern map boundary is most likely due to shallow pre-Miocene bedrock. This notion is supported by pre-Tertiary and Eocene exposures to the north and west of the study area. This area is only moderately magnetic, therefore, we infer a mélange-type lithology (phyllite) that forms the lower extent of our modeling as pre-Tertiary basement. This is supported by exposures of the Easton Metamorphic Suite to the west of the Kittitas Valley (MacDonald and Dragovich, 2015). Conversely, lower gravity over the Kittitas Valley indicates a regional thickening of the Eocene and Oligocene sedimentary sections south of Table Mountain to between 4 and 6 km. This thickening is rather abrupt at the range front and matches results of Saltus (1993).

A broad magnetic high spanning Kittitas Valley suggests thicker, normally magnetized basalt under the valley, though the ages and members are not certain. Erosion has changed the thickness of the Sentinel Bluffs Member along the range front, which may account for some of the difference in thickness between the surface and subsurface. However, the model requires additional normally magnetized basalt under Kittitas Valley to account for the observed magnetic high. We currently interpret this extra basalt as rocks of the Teanaway Formation (unit Evt) and this is supported by highly magnetic exposures of basalt of Teanaway Formation immediately north and west of the mapping area (TNF in Figure M1A). However, thicker packages of GRB are also possible.

The gravity low in between the Dead Coyote (DCF) and Dry Creek (DRCF) faults corresponds to greater thicknesses of basin fill and rocks of the Ellensburg Formation between those faults (see contours in Figure M1A).

INTERPRETATIONS RELATED TO THE GROUSE CREEK MEMBER

Though the Grouse Creek member (unit Mvgg) is at the N2/R2 MSU magnetic boundary (Riedel and Tolan, 2013), we infer that in the map area it is normally magnetized or retains little to no remanent reverse magnetization because magnetic anomalies are moderate (~-200 nT) where it is exposed at higher elevations north of the valley (green colors along GCSH label in Figure M1A). This region of moderate magnetic anomalies is collocated with a relative gravity low (see especially GCSH in Figure M1B). Unit Mvgg is not less dense than other GRB members, so the source of this local gravity low could be either a prevalence of hyaloclastite or interbedded Ellensburg Formation within the unit (as modeled in Figure M1B). The exact thickness of these layers is weakly constrained, but this interpretation requires greater overall Mvgg thickness where exposed in the range front, which suggests a locally low paleotopography during the eruption of the Grouse Creek member. The notion of a paleotopographic low is supported by geologic data: sandstone, pumiceous siltstone, and hyaloclastite form in areas of low topography such as a basin, lake, or river system. The north end of this presumed paleotopographic low is bounded by two short, distinct, gravity gradients (marked by arrows on middle panel of Figure M1B). Abrupt thickness changes in unit Mvgg across concealed(?) normal faults in this location best fits these gravity gradients.

INTERPRETATIONS RELATED TO NEWLY CHARACTERIZED STRUCTURES

A strong, well-mapped, laterally extensive gravity gradient trending west–northwest marks the Dead Coyote fault at the northern edge of the Ellensburg North quadrangle. This gradient supports reverse faulting on a north-dipping fault with an anticline in its hanging wall. A major thickness change in the Ellensburg Formation across the fault, combined with escarpments in units QRcg and Qaf3, suggests that the fault was active in the Miocene, through the Pliocene, into the Quaternary, and is possibly still active. Paired with a linear magnetic low immediately to its north, this suggests reversely-magnetized basalt close to the surface. A magnetic low originates from the reversely magnetized Wapshilla Ridge Member where that unit is uplifted close to the surface and forms the Dead Coyote anticline (DCA). The shape of the anomalies is impossible to model using basalts of CRBG with relatively consistent thickness and a single fold. Therefore, the geophysics strongly supports a backthrust (Figure M1B). An anticline bounded by normal faults is not permissible because the predicted magnetic low would be too small in amplitude and too wide to fit the data. The potential-field data supports small-scale faulting in the center of the anticline, though geometry is poorly constrained.

The shape of the potential-field anomalies north of the Dead Coyote fault strongly supports a concealed asymmetric syncline. Thinning of the Sentinel Bluffs members over the anticline indicates that the anticline was actively forming during the eruption of those units. However, adjusting the thicknesses of the Grouse Creek member and the N1 MSU of the GRB could indicate the fold was active throughout the eruption of the GRB. The vertical separation of the top of the basalt along the DCF is approximately 140 ft, but total slip is poorly constrained given the uncertainty in the precise geometry and dip of the fault. Small-scale faults in the center of the anticline displace the top of the basalt at least ~250 ft in the same sense as the DCF.

A paired magnetic and gravity low south of the DCF strongly supports the thickest near-surface sediment in the geophysical model. The southern edge of this low is marked by a gradient coincident with the DRCF. This gradient is lower amplitude than the DCF gradient, so less offset is indicated on the DRCF, but near-surface changes in sediment thickness suggest recent activity. Deeper in the model, offsets along the DRCF help fit the magnetic data, but several geometries are possible and therefore dip magnitudes and fault offsets are less certain with depth. Aside from near the intrabasinal faults, the near surface sediments have consistent thickness across the Kittitas Valley, and therefore suggest similar recent vertical offsets on faults bounding both the north and south edges of the basin.

DESCRIPTION OF STRUCTURES

This year's mapping newly identifies, characterizes, and refines the locations of geologic structures including reverse faults and short-hinged and long-hinged folds. Mapped faults include the

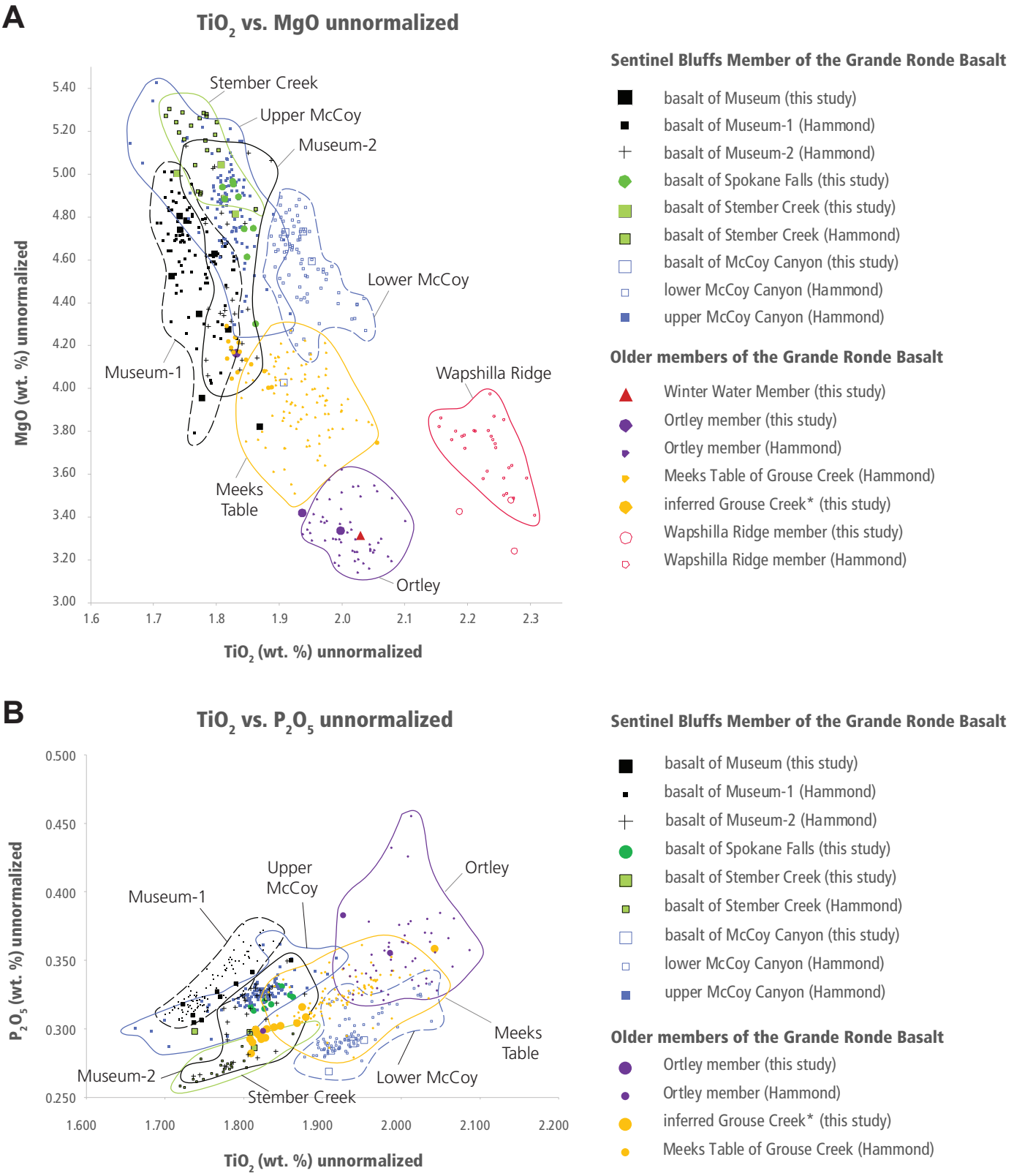

Figure 1. Figure 1A (above) TiO_2 versus MgO plot and Figure 1B (below) TiO_2 versus P_2O_5 plot. Geochemical plots of unnormalized data from this study and from Hammond (2013). Larger symbols are results from this study and smaller symbols are Hammond's data. Geochemical fields are hand-drawn according to data from Hammond (2013). WSU's Machine Learning (ML) model provided classifications for our samples and the geochemical diagrams above help support those classifications. Where fields are absent—Spokane Falls and Winter Water compositions—geochemical compositions of these types were not observed in Hammond's map area. In these cases, only the ML model classified the geochemical results. Where our samples reside in overlapping or between proximal fields, the ML model classifications and stratigraphic considerations are taken into account for our published classification. Note: upper and lower McCoy Canyon of Hammond are grouped as basalt of McCoy Canyon in our study, and Museum-1 (lower) and Museum-2 (upper) are grouped as basalt of Museum in our study. *samples with low confidence ML classifications

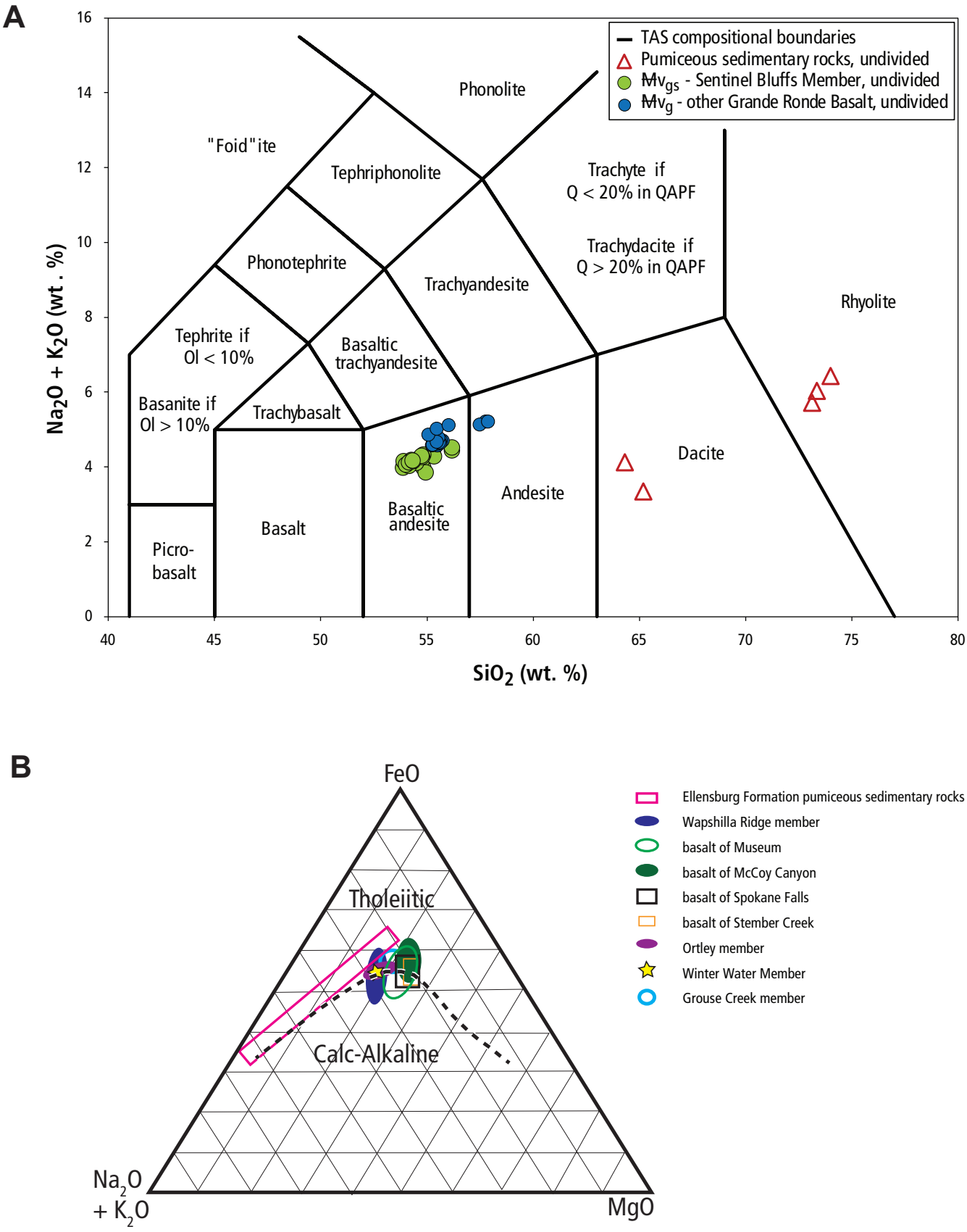

Figure 2. Whole rock geochemistry for volcanic and pumiceous sedimentary rocks in and around the map area. **A.** Total alkali versus silica (TAS) diagram (Le Bas and others, 1986) for selected samples, where most GRB (blue dots) are basaltic andesite and all Sentinel Bluffs Member samples are basaltic andesite (green dots). **B.** AFM diagram (Irvine and Baragar, 1971; Graham and Midgley, 2000) comparing calc-alkaline versus tholeiitic series delineated by a dashed black line, where sample compositions cluster into colored fields.

Dead Coyote fault (DCF), its unnamed backthrust, the Dry Creek fault (DRCF), the Craigs Hill fault, and other minor escarpments and concealed faults. Short-hinged folds include the Dead Coyote anticline (DCA) and unnamed synclines and the long-hinged Kittitas Valley syncline in the basin. Long-hinged monoclines include the Reecer Canyon monocline (RCM) and Wilson Creek monocline (WCM).

Dead Coyote Fault (DCF) and its Backthrust

The DCF is a newly mapped west-striking fault that crosses the northern portion of the Ellensburg North quadrangle. The DCF forms clear escarpments through glacial unit Qapo$_{ks}$ and alluvial units QRcg and Qaf$_3$, with consistently higher elevations (less than ~30 ft) north of the fault. Escarpment heights shrink westward and are unclear beyond the western map boundary, but may continue concealed at depth. Escarpments continue eastward, at least to the map boundary, where they may connect with other faults in the adjacent quadrangle. Observations from a paleoseismic trench "Dead Coyote trench" on unit QRcg (significant site S01) in an unpublished USGS report lists ~2 ft of soil underlain by basaltic bedrock (B. Sherrod, USGS, oral commun., 2019). Fault activity from the paleoseismic excavation is unreported as of 2020. Notably, escarpments related to the DCF on the older unit QRcg are subtler than those on the younger surfaces and may suggest that these subtler escarpments have experienced more erosion, are older, and (or) are less active.

Measurements of fault surfaces and kinematic indicators suggest that the DCF is north-side-up/south-side-down, mostly dip-slip, and steeply (~60°) north-dipping at the surface. Slickenlines on a DCF surface (geochemistry site G51) are oriented 77 degrees from east within the plane of the fault and suggest a component of left-lateral slip, making the DCF an oblique-slip, sinistral, reverse fault. GPS data showing northeast-directed strain also suggest components of sinistral-reverse oblique slip that are consistent with kinematic data on the DCF. It is conceivable that the dip angle decreases with depth to flatten (listric?) and sole into a décollement or into Eocene stratigraphy, possibly making the DCF the shallow portion of a thrust fault. Alternatively, if the dip remains steep with depth or is even near vertical, the DCF may be part of a flower structure in Kittitas Valley. We estimated <500 ft of displacement. Shorter anastomosing synthetic fault strands with comparable to lesser amounts of inferred displacements are north and south of the main strand of the DCF. Notably, an IRSL age on unit Qaf$_3$ (age site GD07, 468.9 ±54.5 ka, Data Supplement Table DS03) north of geochemistry site G51 near the mid-segment of the main fault strand suggests middle Pleistocene age of offset (or younger) for the DCF.

We infer a concealed unnamed fault near a portion of a previously mapped northwest-striking concealed fault (Tabor and others, 1982). This unnamed fault is north of and sub-parallel to the DCF, and inferred to be south-dipping and south-side-up, thus making it antithetic to the DCF. The amount of dip on this fault is unclear, and inferred to be high angle (45–90°) based on our models. We interpret this fault to be a backthrust to the DCF that obliquely bounds the northeast limb of an anticline. A significant aeromagnetic gradient showing magnetic lows to the south and magnetic highs to the north help delineate its extent to the east and west (Figure M1A). We estimate <350 ft of displacement on the backthrust. From aeromagnetic anomalies we interpret concealed fault intersections among the DCF, its backthrust, and other faults north of the bend in Cross Section A–A′ and south of geochemistry site G12.

Dry Creek Fault (DRCF)

The DRCF was named by Bentley (1977), previously mapped by Bentley (1977) and Waitt (1979), and also referred to as the Reecer Creek fault by Blakely and others (2011). It is a concealed east-striking fault that spans the entire width of the map area for at least ~6.8 miles. In the eastern map area, Waitt (1979) identified a ~150-ft high scarp that offsets gravel deposits of unit QRcg. In the central map area, it is identified by a west-trending series of at least six knolls (less than 30 ft tall) of Quaternary outwash and Quaternary to Pliocene alluvium that have tall, steep, north-facing slopes and gentle, south-facing slopes. We infer this fault to be a reverse-to-thrust fault with south-side-up/north-side-down slip and a moderate to steep south dip that is possibly listric. It is possible that the DRCF represents a fault tip splay associated with the Frenchman Hills thrust farther east. Future mapping will help assess this hypothesis. We estimate 100–350 ft of displacement. It is likely responsible for the significant height difference between the high terrace of unit Rcg on the eastern map area and south of the North Branch canal, where the south side is ~2,150-ft elevation and the north side is ~2,000-ft elevation. Our mapping also identifies low topographic breaks on the knolls south of the DRCF, interpreted to be a questionable splay of faults that may be antithetic to the DRCF.

Craigs Hill Fault

The east-striking Craigs Hill fault is entirely concealed in the map area north of its namesake (a long, narrow hill in the southeastern portion of the map area that continues off the map southward). It was previously identified by Waitt (1979) from a series of 15 knolls of unit QRcg elevated above the valley floor, where the Craigs Hill fault is concealed north of the knolls, suggesting a south-side-up geometry. It is inferred to be a south-dipping, reverse and (or) high-angle fault with north-side-down/south-side-up offset. It continues farther east outside of the map area and may be the western continuation of the Frenchman Hills thrust located farther east. More work will need to be done to assess this notion. In the opposite direction, it is probable that the Craigs Hill fault extends farther west to the map boundary and beyond, because a weak gravity anomaly is observed where the fault projects westward to intersect Cross Section A–A′. If it is present, the fault may have displacements too small to be resolved by potential-fields data. The Craigs Hill fault may also be related to the frontal fault of Manastash Ridge farther south, and if so, it may be a young thrust.

Concealed Minor Faults

Concealed faults identified from geologic data or geophysical interpretation:

- Conspicuously straight north-northwest- and north-northeast-trending canyons may contain concealed strike-slip faults as identified from offset contacts of the Coleman member or the basalt of McCoy Canyon (Reecer Canyon, Currier Canyon, etc). Total displacements for these strike-slip faults may be considerable and carry implications for (1) palinspastic reconstruction of this portion of the YFTB, and (2) accommodation space considerations for GRB emplacement. Northeast- and northwest-striking, strike-slip "cross faults" are reported in the YFTB to the south of the map area (Anderson and others, 2013), and our aforementioned concealed minor faults reflect a similar geometry possibly related to transpression or transtension and possibly responsible for producing several straight canyons to the north of Kittitas Valley. Geologic evidence for a north-northwest-striking, strike-slip fault along Wilson Creek is unclear, but cannot be ruled out given the creek's straightness over a long distance.
- In the northern map area, two west-northwest-trending geophysical gradients (faults near 'GCSH' label in Figure M1B) may represent re-activated Eocene, basin-bounding, normal-oblique(?) faults formed from regional transtension and Eocene strike-slip faulting possibly driven by oblique subduction (Johnson, 1985) and reactivated by regional extension related to Miocene eruptions from the Yellowstone Hot Spot (YHS). We infer that these faults were either active (1) before Miocene clockwise rotation and compression initiated, and (or) (2) while compression associated with clockwise rotation of the Pacific Northwest competed against regional extension related to the YHS. Our cross section and geophysical modeling suggest shortening began predominantly during the eruption of the Sentinel Bluffs. Staisch and others (2018a) show reactivated normal faults near Umtanum and Manastash Ridges to the south of the map area, which suggests that Kittitas Valley may also have reactivated normal faults elsewhere at depth.
- From geophysical anomalies we interpret a concealed fault north of the backthrust and in the southeast area of the Reecer Canyon quadrangle. Numerous escarpments of unknown origin also help constrain the position and south-side-down sense of slip for a short segment of a questionable concealed fault. Note that escarpments of unknown origin may be: (a) CRBG flow breaks, (b) incipient landslide headscarps, (c) mass-wasting related to seasonal freeze-thaw, or (d) faults. Forward modeling of our geophysical data also suggests the possibility of a concealed north-dipping thrust fault between DCF and DRCF. If it exists, then it may intersect with the DCF at depth.

Dead Coyote Anticline

The DCA is characterized as a short-hinged (~7,000-ft long), northwest-plunging anticline located between the DCF and its backthrust. The DCA has an interlimb angle of ~145 degrees, is gentle, upright, slightly south-verging, and probably symmetric. The DCA contains basalt of Stember Creek or older McCoy Canyon in its core at the surface, and is inferred to be a fault-propagation fold related to the DCF. Thinning of Sentinel Bluffs members on the anticline suggest uplift and erosion during Sentinel Bluff-time, whereas mildly constrained but consistent thicknesses of the Wapshilla Ridge Member across the fold as geophysically modeled suggest no concomitant folding during Wapshilla Ridge-time. Folding may have occurred after eruption of the Wapshilla Ridge Member, possibly at the same time as the eruption of the Sentinel Bluffs Member.

Basin Synclines

The previously mapped (Tabor and others, 1984) southeast-plunging Kittitas Valley syncline is concealed in the southwestern map area. This long-hinged syncline spans the entirety of the long-axis of Kittitas Valley, off-center and closer to the southern range front of Manastash Ridge. We infer that the Kittitas Valley syncline is structurally controlled in some way, likely related to development of the Yakima fold and thrust belt, and may be gentle-to-open and upright to slightly northeast-verging. Near and along its axis, we infer thicker packages of bedrock and basin fill.

A long, unnamed, concealed syncline is inferred south of the range front and north of the DCA from opposing dips of Sentinel Bluffs members. Geophysical modeling suggests thicker GRB in this syncline and suggests it is slightly asymmetric with a slightly steeper south limb. Asymmetry may be attributed to proximity to the DCF backthrust and associated deformation.

Reecer Canyon Monocline and Wilson Creek Monocline

The Reecer Canyon (RCM) and Wilson Creek (WCM) monoclines are identified by subtle and very gradual changes in dip of flow foliations on basalt outcrops of unit Mvgg in the northern map area, and based on geophysical modeling. The RCM and WCM both trend northwest, sub-parallel to one another, and together may form a structural terrace. They are long-hinged, low-amplitude, south-verging monoclines where the inflection points of their anticlinal fold hinges are mapped broadly and are only approximately located (for example, long-wavelength folds can have poorly located hinge lines where the density of orientation measurements is low).

The monoclines span the width of the northern map area, end westward into the Eocene stratigraphy (unit Evt), and merge eastward outside the map area. Arguably, these two monoclines may be a single monocline given the dip changes gradually (~0°–29°) over a large area within the Grouse Creek member, and the notion that flow foliations contain inherent local variability due to heterogeneities in cooling lava at outcrop scale (this intrinsic variability is greatly reduced to absent in bedding). However, geophysical modeling suggests two subtle ramps in the Grouse Creek member at depth.

The RCM and WCM are likely fault-related folds and possibly fault-cored by one or more compressional faults. The RCM is proximal to a north-dipping reverse fault ("facet fault" north of geochemistry site G46) and thereby may be a fault-related monocline. Similarly, the WCM is collocated with segments of the concealed re-activated normal faults that are suggested by geophysical modeling. Miocene and younger deformation may be transferring from brittle reactivation of concealed Eocene structures to tilting and folding of the Grouse Creek member.

Alternatively, the folds may be related to a deep, gently dipping thrust fault concealed beneath Table Mountain, of which the DCF and "facet fault" are its surface expressions. This gently dipping fault hypothesis is equally plausible as the steeply dipping fault hypothesis reflected on Cross Section A–A′. In either hypothesis, we interpret folding with concomitant faulting, where most of the shortening is accommodated by folding before (Kelsey and others, 2017) and during fault-propagation, and occurring during and after the eruption of the GRB.

DISCUSSION

Miocene Evolution of Kittitas Basin

Interpreted geologic history of the map area from Miocene to present:

1. Lavas of Wapshilla Ridge erupted over older GRB units that incompletely filled the Eocene-aged(?) transtensional Kittitas basin. These lavas covered the then low-lying northern range front, and proceeded northward onto Eocene rocks at the northern extent of the CRBG (near the northern map area) to the Eocene basin boundary.

2. Lavas of Grouse Creek erupted into a Miocene paleotopographic low where the present range front is located and encountered a lake or river to produce hyaloclastite and peperite.

3. A short quiescence in volcanism allowed sedimentary rocks of the Coleman member to deposit in and around the same Miocene low that the Grouse Creek lavas were filling.

4. Eruption of GRB lavas resumed primarily with lavas of Sentinel Bluffs and continued to fill the Kittitas basin and areas farther north.

5. Possibly during the eruption of some GRB units and certainly after the eruption of the Sentinel Bluffs lavas, regional clockwise rotation and concomitant compression began, resulting in these units being uplifted, eroded, and thinned.

6. By the time of the eruption of the Saddle Mountains lavas, the current location of the northern range front had established itself, and Kittitas Valley deepened while the Yakima Folds formed ridges to the north and south.

7. Post-CRBG sedimentation continued to fill Kittitas basin with the upper Ellensburg Formation, Thorp Gravels, glacial outwash, and alluvial fans.

Natural Hazards and Water Resources

The most common natural hazards in the map area are landslides and other mass-wasting events, including debris flows on young alluvial fan surfaces. Considerable landslide hazards exist along cliffs of deep canyons in the northern map area, along the frontal range front to south of the faceted spurs, and downslope from and in close proximity to the Coleman member. Debris flow hazards are also possible in the lowlands, particularly on younger alluvial fan units Qaf$_2$, Qaf$_1$, Qia, and Qa. Great care should be taken when constructing buildings or infrastructure near or on these surfaces.

Seismic hazards related to the DCF may be possible given its considerable length, connection to larger faults, and relatively young age (Pleistocene ~500 ka, IRSL site GD07). Recurrence, slip rate, and amount of slip are currently unknown. Further research is planned to assess the activity of this fault (S. Angster, USGS, oral commun., 2020) with a proposed paleoseismic trench to be located west of Reecer Creek Road. Focal mechanism calculations from historic earthquakes (1978–2018) near the Kittitas basin show a range of magnitudes (Md or Ml) from 1.0 to 4.2. The mean magnitude of 99 events is 2.46 ±1.24 (2σ), and about two-thirds have a reverse or oblique-reverse sense of slip (R. Cakir, WGS, written commun., 2019). Calculated focal mechanisms are generally outside of the map area to the west and to the southeast, and the most proximal cluster of events is near the Boylston Mountains to the southeast. No focal mechanisms are calculated on faults within the map area. The closest earthquake with a focal mechanism is located near Table Mountain and is a local magnitude 2.7 exhibiting oblique-reverse slip. However, earthquakes without focal mechanism calculations have epicenters that cluster near the DCF and DRCF with small magnitudes (2.0–3.0), whereas other single events are located near the planned USGS trench and near the head of Currier Canyon (Pacific Northwest Seismic Network, 2020).

The Coleman member within the DCA may serve as a potential shallow aquifer. The member lies in a classic anticlinal structural trap confined above and below by GRB and north and south by compressional faults. Drilling for water resources within the hanging walls of these faults away from the anticlinal crest may prove useful and economical for future groundwater supply. The sedimentary interbeds in the syncline north of the anticline may also contain additional economically accessible water resources.

RECOMMENDATIONS FOR FUTURE RESEARCH

- **Refining alpine glacial histories**—Careful investigation of landforms and unconsolidated deposits in the northern half of the Reecer Canyon quadrangle and areas north of there will help delineate the extent of alpine glaciation and elucidate the origin of monomict unconsolidated deposits.
- **Assessing hyaloclastites**—Whole rock geochemistry samples of glass fragments from hyaloclastite units may elucidate eruption histories and magmatic processes of the upper GRB. U-Pb analysis of hyaloclastite material may prove insightful for constraining age relationships. Additional mapping of hyaloclastites may have paleotopographic implications for ancient courses of Miocene rivers of the Pacific Northwest.
- **Comparing gravel units**—Two new U-Pb analyses of detrital zircons (age site GD05 and GD06) reported here establish clear provenance spectra from the "Naneum Gravel" (unit QRcg). Comparing provenances of these data in the eastern map area to those of the Thorp Gravel in the western map area may refine the temporal relationship between units QRcg and Rcgt. Additional U-Pb analyses

of detrital zircons from interbedded ashes, sands, and finer matrix material within the Thorp Gravel (unit Rcgt) will be necessary for a comparison.

- **Clarifying Grande Ronde stratigraphy**—Additional systematic collection of whole rock geochemistry samples from basaltic andesite above and below the Coleman member will clarify how the Ortley, Winter Water, and lower Sentinel Bluffs members pinch out relative to the sedimentary unit, and may inform our understanding of Miocene paleotopography.
- **Elucidating pre-12 Ma regional deformation**—The deformational history is unclear for a period of time before the ~12 Ma onset of compression/transpression that is responsible for the Yakima fold and thrust belt, and after the cessation of Eocene extension/transtension responsible for sedimentary basin development. Additional paleomagnetic samples from well-exposed GRB outcrops present opportunities to inform regional deformational histories before the onset of regional clockwise rotation circa 12 Ma.

ACKNOWLEDGMENTS

We thank Nick Zentner, Andy Miner, Chris Mattinson, Angela Halfpenny, and Logan Wetherell of Central Washington University (CWU) for many hours of meaningful conversations and field trips; CWU graduate students Valerie Strasser, for her insightful assistance with geochemical data, and Silas Sleeper, for subsurface well data discussions and data sharing; Washington Geological Survey staff Alex Steely, Will Gallin, Michael Polenz, and Cat Samson for insightful reviews of findings; Steve Angster, Brian Sherrod, Lydia Staisch, and Ralph Haugerud of USGS for help synthesizing past and on-going regional work, and Wendy Welch for sharing legacy subsurface interpretations; emeritus investigators Jack Powell, Steve Reidel, Terry Tolan, and Richard Waitt for passing the torch and clarifying stratigraphic questions; John Wolff and the whole staff at the Washington State University Peter Hooper GeoAnalytical lab in Pullman, WA for analyzing geochemistry samples and classifying CRBG rocks using their Machine Learning (ML) model; Chris Pitre of Coho Water Resources, Carl Carlson III of Carlson Brothers Jewelry Tacoma, WA, Wes Engstrom, Steve Zebransky, and Rob Repin of Liberty, WA for access to property and introducing me to their ideas surrounding the Ellensburg Blue agates; the Watkins, Wakefield, Lund, and other families along with countless other private landowners and businesses for land access; Joe Sherrod of the University of Washington for his insightful graduate work east of the map area; and Happy's Market for their delicious belly-filling breakfast burritos.

REFERENCES

Aitken, M. J., 1998, An introduction to optical dating: The dating of Quaternary sediments by the use of photon-stimulated luminescence: Oxford University Press, 267 p.

Aitken, M.J.; Xie, Jun, 1990, Moisture correction for annual gamma dose: Ancient TL, v. 8, no. 2, p. 6–9.

Allmendinger, R. W.; Cardozo, Nestor; Fisher, D. M., 2012, Structural geology algorithms: Vectors and tensors: Cambridge University Press, 289 p.

Anderson, Tom, 2002, Correction of common lead in U-Pb analyses that do not report ^{204}Pb: Chemical Geology, v. 192, no. 1–2, p. 59–79. [https://doi.org/10.1016/S0009-2541(02)00195-X]

Anderson, J. L.; Tolan, T. L.; Wells, R. E., 2013, Strike-slip faults in the western Columbia River flood basalt province, Oregon and Washington. *In* Reidel, S. P.; Camp, V. E.; Ross, M. E.; Wolff, J. A.; Martin, B. S.; Tolan, T. L.; Wells, R. E., editors, The Columbia River flood basalt province: Geological Society of America Special Paper 497, p. 325–347. [https://doi.org/10.1130/2013.2497(13)]

Auclair, Marie; Lamothe, Michel; Huot, Sébastien, 2003, Measurement of anomalous fading for feldspar IRSL using SAR: Radiation Measurements, v. 37, no. 4–5, p. 487–492. [https://doi.org/10.1016/S1350-4487(03)00018-0]

Bentley, R. D., 1977, Stratigraphy of the Yakima basalts and structural evolution of the Yakima ridges in the western Columbia Plateau. *In* Brown, E. H.; Ellis, R. C., editors, Geology excursions in the Pacific Northwest: Geological Society of America, p. 339–390.

Blakely, R. J.; Sherrod, B. L.; Weaver, C. S., 2020a, High-resolution aeromagnetic survey of the Wenatchee area, Washington: U.S. Geological Survey data release. [https://doi.org/10.5066/P9EURKIG]

Blakely, R. J.; Sherrod, B. L.; Weaver, C. S., 2020b, High-resolution aeromagnetic survey of the Cle Elum area, Washington: U.S. Geological Survey data release. [https://doi.org/10.5066/P9C9MADW]

Blakely, R. J.; Sherrod, B. L.; Weaver, C. S.; Wells, R.E.; Rohay, A. C., 2014, The Wallula fault and tectonic framework of south-central Washington, as interpreted from magnetic and gravity anomalies: Tectonophysics, v. 624–625, p. 32–45. [https://doi.org/10.1016/j.tecto.2013.11.006]

Blakely, R. J.; Sherrod, B. L.; Weaver, C. S.; Wells, R. E.; Rohay, A. C.; Barnett, E. A.; Knepprath, N. E., 2011, Connecting the Yakima fold and thrust belt to active faults in the Puget Lowland, Washington: Journal of Geophysical Research Solid Earth, v. 116, no. B7, p. 1–33. [https://doi.org/10.1029/2010JB008091]

Brocher, T. M.; Wells, R. E.; Lamb, A. P.; Weaver, C. S., 2017, Evidence for distributed clockwise rotation of the crust in the northwestern United States from fault geometries and focal mechanisms: Tectonics, v. 36, no. 5, p. 787–818. [https://doi.org/10.1002/2016TC004223]

Cardozo, Nestor; Allmendinger, R. W., 2013, Spherical projections with OSXStereonet: Computers & Geosciences, v. 51, p. 193–205. [https://doi.org/10.1016/j.cageo.2012.07.021]

Chiba, Tatsuro; Kaneta, Shin-ichi; Suzuki, Yusuke, 2008, Red relief image map: New visualization method for three dimensional data: The International Archives of the Photogrammetry, Remote Sensing and Spatial Information Sciences, v. 37, no. B2, p. 1071–1076.

Czajkowski, J. L.; Bowman, J. D.; Schuster, J. E.; Wheeler, C. M., 2012, Oil and gas wells in Washington State: Washington Division of Geology and Earth Resources Open File Report 2012-02 (rev. 2015), 4 p., 1 Microsoft Excel file with 4 p. text. [http://www.dnr.wa.gov/Publications/ger_ofr2012-02_oil_and_gas_wells.zip]

Ebinghaus, Alena; Jolley, D. W.; Hartley, A. J., 2015, Extrinsic forcing of plant ecosystems in a large igneous province: The Columbia River flood basalt province, Washington State, USA: Geology, v. 43, no. 12, p. 1107–1110. [https://doi.org/10.1130/G37276.1]

Eddy, M. P.; Bowring, S. A.; Umhoefer, P. J.; Miller, R. B.; McLean, N. M.; Donaghy, E. E., 2016, High-resolution temporal and stratigraphic record of Siletzia's accretion and triple junction migration from nonmarine sedimentary basins in central and western Washington: Geological Society of America Bulletin, v. 128, no. 3–4, p. 425–441. [https://doi.org/10.1130/B31335.1]

Eddy, M. P.; Umhoefer, P. J.; Miller, R. B.; Donaghy, E. E.; Gundersen, Melissa; Senes, F. I., 2017, Sedimentary, volcanic, and structural processes during triple-junction migration: Insights from the Paleogene record in central Washington. *In* Haugerud, R. A.; Kelsey, H. M., editors, From the Puget Lowland to east of the Cascade Range: Geologic Excursions in the Pacific Northwest: Geological Society of America Field Guide 49, p. 143–174.

FEMA, 2011, Kittitas FEMA 2011 project, collected between Apr. 17 and Apr. 19, 2011 by Watershed Sciences, Inc., 6-ft resolution, accessed Aug. 31, 2020 [http://lidarportal.dnr.wa.gov/], metadata available on portal [ger_kittitas_fema_2011_lidar_report.pdf].

Galbraith, R. F.; Roberts, R. G., 2012, Statistical aspects of equivalent dose and error calculation and display in OSL dating: An overview and some recommendations: Quaternary Geochronology, v. 11, p. 1–27. [https://doi.org/10.1016/j.quageo.2012.04.020]

Graham, D. J.; Midgley, N. G., 2000, Graphical representation of particle shape using triangular diagrams: An Excel spreadsheet method: Earth Surface Processes and Landforms, v. 25, no. 13, p. 1473–1477. [https://doi.org/10.1002/1096-9837(200012)25:13<1473::AID-ESP158>3.0.CO;2-C]

Guérin, Guillaume; Mercier, Norbert; Adamiec, Grzegorz, 2011, Dose-rate conversion factors: Update: Ancient TL, v. 29, no. 1, p. 5–8.

Hammond, P. E., 2013, Distribution, stratigraphy, and structure of the Grande Ronde Basalt in the upper Naches River basin, Yakima and Kittitas Counties, Washington. *In* Reidel, S. P.; Camp, V. E.; Ross, M. E.; Heiskanen, W. A.; Meinesz, F. A. V., 1958, Earth and its gravity field: McGraw-Hill, 470 p.

Hollocher, Kurt; Robinson, Peter; Walsh, Emily; Roberts, David, 2012, Geochemistry of amphibolite-facies volcanics and gabbros of the Støren Nappe in extensions west and southwest of Trondheim, western gneiss region, Norway: A key to correlations and paleotectonic settings: American Journal of Science, v. 312, no. 4, p. 357–416. [https://doi.org/10.2475/04.2012.01]

Hoyt, C. L., 1961, The Hammond sill—An intrusion in the Yakima Basalt near Wenatchee, Washington: Northwest Science, v. 35, no. 2, p. 58–64.

Huang, Lei; Liu, Chi-yang, 2017, Three types of flower structures in a divergent-wrench fault zone: Journal of Geophysical Research Solid Earth, v. 122, no. 12, p. 10,478–10,497. [https://doi.org/10.1002/2017JB014675]

Huntley, D. J.; Baril, M. R., 1997; The K content of the K-feldspars being measured in optical dating or in thermoluminescence dating: Ancient TL, v. 15, no. 1, p. 11–13.

Huntley, D. J.; Hancock, R. G. V., 2001; The Rb contents of the K-feldspar grains being measured in optical dating: Ancient TL, v. 19, no. 2, p. 43–46.

Huntley, D. J.; Lamothe, Michel, 2001, Ubiquity of anomalous fading in K-feldspars and the measurement and correction for it in optical dating: Canadian Journal of Earth Sciences, v. 38, no. 7, p. 1093–1106. [https://doi.org/10.1139/e01-013]

Irvine, T. N.; Baragar, W. R. A., 1971, A guide to the chemical classification of the common volcanic rocks: Canadian Journal of Earth Sciences, v. 8, no. 5, p. 523–548. [https://doi.org/10.1139/e71-055]

Jachens, R. C.; Roberts, C. R., 1981, Documentation of a FORTRAN program, 'isocomp', for computing isostatic residual gravity: U.S. Geological Survey Open-File Report 81-574, 26 p. [https://doi.org/10.3133/ofr81574]

Jackson, S. E.; Pearson, N. J.; Griffin, W. L.; Belousava, E. A., 2004, The application of laser ablation-inductively coupled plasma-mass spectrometery to in situ U-Pb zircon geochronology, Chemical Geology, v. 211, p. 47–69. [https://doi.org/10.1016/j.chemgeo.2004.06.017]

Johnson, S. Y., 1985, Eocene strike-slip faulting and nonmarine basin formation in Washington. *In* Biddle, K. T.; Christie-Blick, Nicholas, editors, Strike-slip deformation, basin formation, and sedimentation: Society of Economic Paleontologists and Mineralogists Society for Sedimentary Geology Special Publication 37, p. 283–302. [https://doi.org/10.2110/pec.85.37.0265]

Jones, M. A.; Vaccaro, J. J., 2008, Extent and depth to top of basalt and interbed hydrogeologic units, Yakima River basin aquifer system, Washington: U.S. Geological Survey Scientific Investigations Report SIR 2008-5045, 22 p. [http://pubs.usgs.gov/sir/2008/5045]

Jones, M. A.; Vaccaro, J. J.; Watkins, A. M., 2006, Hydrogeologic framework of sedimentary deposits in six structural basins, Yakima River basin, Washington: U.S. Geological Survey Scientific Investigations Report 2006-5116, 24 p., 7 plates, scales 1:100,000 and 1:200,000. [http://pubs.usgs.gov/sir/2006/5116/]

Kaatz, M. R., 1959, Patterned ground in central Washington; A preliminary report: Northwest Science, v. 33, no. 4, p. 145–156.

Kasbohm, Jennifer; Schoene, Blair, 2018, Rapid eruption of the Columbia River flood basalt and correlation with the mid-Miocene climate optimum: Science Advances, v. 4, no. 9, 8 p. [https://doi.org/10.1126/sciadv.aat8223]

Kelsey, H. M.; Ladinsky, T. C.; Staisch, Lydia; Sherrod, B. L.; Blakely, R. J.; Pratt, T. L.; Stephenson, W. J.; Odum, J. K.; Wan, Elmira, 2017, The story of a Yakima fold and how it informs late Neogene and Quaternary backarc deformation in the Cascadia subduction zone, Manastash anticline, Washington, USA: Tectonics, v. 36, no. 10, p. 2085–2107. [https://doi.org/10.1002/2017TC004558]

Kittitas County, 2012, Manastash Creek 2012 project, collected on May 7, 2012 by 3Di Herrera, Inc., 3-ft resolution, accessed Aug. 31, 2020 [http://lidarportal.dnr.wa.gov/], data available on portal [ger_manastash_creek_2012_lidar_report.pdf].

Lamb, Jodie, 1997, Quaternary stratigraphy of the Kittitas Valley, with emphasis on the Craigs Hill section: Central Washington University Senior thesis, 96 p.

Le Bas, M. J.; LeMaitre, R. W.; Streckeisen, Albert; Zanettin, Bruno, 1986, A chemical classification of volcanic rocks based on the total alkali-silica diagram: Journal of Petrology, v. 27, no. 3, p. 745–750. [https://doi.org/10.1093/petrology/27.3.745]

Ludwig, K. R., 2003, User's manual for Isoplot 3.00: A geochronological toolkit for Microsoft Excel: Berkeley Geochronology Center, Special Publication no. 4a, Berkeley, California.

Mabry, J. J., 2000, Field trip guidebook to the natural history of Kittitas County: Central Washington University Media Department Press, 73 p.

Macdonald, J. H. Jr.; Dragovich, J. D., 2015, Sedimentary geochemistry of the Peshastin Formation and Darrington Phyllite, Cascade mountains, Washington State: Provenance, tectonic setting, and regional implications: Geological Society of America Special Paper 513, p. 441–460. [https://doi.org/10.1130/2015.2513(12)]

McCaffrey, Robert; King, R. W.; Payne, S. J.; Lancaster, Matthew, 2013, Active tectonics of northwestern U. S. inferred from GPS-derived surface velocities: Journal of Geophysical Research Solid Earth, v. 118, no. 2, p. 709–723. [https://doi.org/10.1029/2012JB009473]

McDonald, E. V.; Busacca, A. J., 1992, Late Quaternary stratigraphy of loess in the Channeled Scabland and Palouse regions of Washington State: Quaternary Research, v. 38, no. 2, p. 141–156. [https://doi.org/10.1016/0033-5894(92)90052-K]

McMillan, Kent; Long, P. E.; Cross, R. W., 1989, Vesiculation in Columbia River Basalts. *In* Reidel, S. P.; Hooper, P. R., editors, Volcanism and tectonism in the Columbia River flood-basalt province: Geological Society of America Special Paper 239, p. 157–167. [https://doi.org/10.1130/SPE239-p157]

Mejdahl, Vagn, 1979. Thermoluminescence dating: Beta-dose attenuation in quartz grains: Archaeometry, v. 21, p. 61–72.

Morelli, Carlo; Gantar, C.; Honkasalo, Tauno; McConnel, R. K.; Tanner, J. G.; Szabo, Bela; Uotila, Urho; Whalen, C. T., 1974, The international gravity standardization net 1971 (IGSN71): International Association of Geodesy Special Publication No. 4, 194 p.

Owens, Ron, 1995, The hydrology of the Kittitas Valley, Washington: Central Washington University Master of Science thesis, 205 p., 6 plates.

Pacific Northwest Seismic Network, 2020, Recent Earthquakes List [database]: Pacific Northwest Seismic Network. [accessed Aug. 15, 2020 at https://pnsn.org/earthquakes/map?city_center=&custom-ui=rectangle&date_end=2020-8-15&date_start=1969-2-14&depth_max=1000&depth_min=-5&distance=&etypes%5B%5D=le&etypes%5B%5D=uk&etypes%5B%5D=re&etypes%5B%5D=lf&gap_max=&lat_center=&lat_max=47.2837&lat_min=46.83652&lon_center=&lon_max=-119.95917&lon_min=-120.74194&mag_max=10&mag_min=-2&order=desc&phase_min=&radius=&rms_max=&s_phase_min=&sort_by=event_time_utc]

Petrus, J. A.; Kamber, B. S., 2012, VizualAge: A novel approach to laser ablation ICP-MS U-Pb geochronology data reduction: Geostandards and Geoanalytical Research, v. 36, no. 3, p. 247–270.

PSLC/WA DNR, 2015, Teanaway 2015 project, collected between Apr. 3 and May 3, 2015 by Quantum Spatial, Inc., 3-ft resolution, accessed Aug. 31, 2020 [http://lidarportal.dnr.wa.gov/], metadata available on portal [ger_teanaway_2015_lidar_report.pdf].

Porter, S. C., 1975, Weathering rinds as a relative-age criterion: Application to subdivision of glacial deposits in the Cascade Range: Geology, v. 3, no. 3, p. 101–104. [https://doi.org/10.1130/0091-7613(1975)3<101:WRAARC>2.0.CO;2]

Porter, S. C., 1976, Pleistocene glaciation in the southern part of the north Cascade Range, Washington: Geological Society of America Bulletin, v. 87, no. 1, p. 61–75. [https://doi.org/10.1130/0016-7606(1976)87<61:PGITSP>2.0.CO;2]

Prescott, J. R.; Hutton, J. T.; 1994; Cosmic ray contributions to dose rates for luminescence and ESR dating: Large depths and long-term time variations: Radiation Measurements, v. 23, no. 2–3, p. 497–500. [https://doi.org/10.1016/1350-4487(94)90086-8]

Rees-Jones, Julie, 1995, Optical dating of young sediments using fine-grain quartz: Ancient TL, v. 13, no. 2, p. 9–14.

Reidel, S. P., 2005, A lava flow without a source: The Cohassett flow and its compositional components, Sentinel Bluffs Member, Columbia River Basalt Group: Journal of Geology, v. 113, no. 1, p. 1–21. [https://doi.org/10.1086/425966]

Reidel, S. P.; Camp, V. E.; Tolan, T. L.; Kauffman, J. D.; Garwood, D. L., 2013b, Tectonic evolution of the Columbia River flood basalt province. *In* Reidel, S. P.; Camp, V. E.; Ross, M. E.; Wolff, J. A.; Martin, B. S.; Tolan, T. L.; Wells, R. E., editors, The Columbia River flood basalt province: Geological Society of America Special Paper 497, p. 293–324. [https://doi.org/10.1130/2013.2497(12)]

Reidel, S. P.; Camp, V. E.; Tolan, T. L.; Martin, B. S., 2013a, The Columbia River flood basalt province: Stratigraphy, areal extent, volume, and physical volcanology. *In* Reidel, S. P.; Camp, V. E.; Ross, M. E.; Wolff, J. A.; Martin, B. S.; Tolan, T. L.; Wells, R. E., editors, The Columbia River flood basalt province: Geological Society of America Special Paper 497, p. 1–44. [https://doi.org/10.1130/2013.2497(01)]

Reidel, S. P.; Scott, G. R.; Bazard, D. R.; Cross, R. W.; Dick, Brian, 1984, Post-12 million year clockwise rotation in the central Columbia Plateau, Washington: Tectonics, v. 3, no. 2, p. 251–273. [https://doi.org/10.1029/TC003i002p00251]

Reidel, S. P.; Tolan, T. L., 2013, The Grande Ronde Basalt, Columbia River Basalt Group. *In* Reidel, S. P.; Camp, V. E.; Ross, M. E.; Wolff, J. A.; Martin, B. S.; Tolan, T. L.; Wells, R. E., editors, The Columbia River flood basalt province: Geological Society of America Special Paper 497, p. 117–154. [https://doi.org/10.1130/2013.2497(05)]

Rosenmeier, F. J., 1968, Stratigraphy and structure of the Table mountain–Mission Peak area in the Wenatchee Mountains, central Washington: University of Washington Master of Science thesis, 44 p., 1 plate.

Saltus, R. W., 1993, Upper-crustal structure beneath the Columbia River Basalt Group, Washington: Gravity interpretation controlled by borehole and seismic studies: Geological Society of America Bulletin, v. 105, no. 9, p. 1247–1259. [https://doi.org/10.1130/0016-7606(1993)105<1247:UCSBTC>2.3.CO;2]

Schmincke, Hans-Ulrich, 1964, Petrology, paleocurrents, and stratigraphy of the Ellensburg Formation and interbedded Yakima Basalt flows, south-central Washington: Johns Hopkins University Doctor of Philosophy thesis, 426 p.

Schmincke, Hans-Ulrich, 1967, Stratigraphy and petrography of four upper Yakima Basalt flows in south-central Washington: Geological Society of America Bulletin, v. 78, no. 11, p. 1385–1422. [https://doi.org/10.1130/0016-7606(1967)78[1385:SAPOFU]2.0.CO;2]

Sherrod, B. L.; Blakely, R. J.; Lasher, J. P.; Lamb, Andrew; Mahan, S. A.; Foit, F. F.; Barnett, E. A., 2016, Active faulting on the Wallula fault zone within the Olympic-Wallowa lineament, Washington State, USA: Geological Society of America Bulletin, v. 128, no. 11–12, p. 1636–1659. [https://doi.org/10.1130/B31359.1]

Smith, G. A., 1988a, Neogene synvolcanic and syntectonic sedimentation in central Washington: Geological Society of America Bulletin, v. 100, no. 9, p. 1479–1492. [https://doi.org/10.1130/0016-7606(1988)100<1479:NSASSI>2.3.CO;2]

Smith, G. A., 1988b, Sedimentology of proximal to distal volcaniclastics dispersed across an active foldbelt: Ellensburg Formation (late Miocene), central Washington: Sedimentology, v. 35, no. 6, p. 953–977. [https://doi.org/10.1111/j.1365-3091.1988.tb01740.x]

Staisch, Lydia; Blakely, Richard; Kelsey, Harvey; Styron, Richard; Sherrod, Brian, 2018a, Crustal structure and Quaternary acceleration of deformation rates in central Washington revealed by stream profile inversion, potential field geophysics, and structural geology of the Yakima folds: Tectonics, v. 37, no. 6, p. 1750–1770. [https://doi.org/10.1029/2017TC004916]

Staisch, Lydia; Kelsey, Harvey; Sherrod, Brian; Moller, Andreas; Paces, James; Blakely, Richard; Styron, Richard, 2018b, Miocene–Pleistocene deformation of the Saddle Mountains: Implications for seismic hazard in central Washington, USA: Geological Society of America Bulletin, v. 130, no. 3–4, p. 411–437. [https://doi.org/10.1130/B31783.1]

Swick, C. H., 1942, Pendulum gravity measurements and isostatic reductions: U.S. Department of Commerce Coast and Geodetic Survey Special Publication 232, 82 p.

Sláma, Jiří; Košler, Jan; Condon, D. J.; Crowley, J. L.; Gerdes, Alex; Hanchar, J. M.; Horstwood, M. S. A.; Morris, G. A.; Nasdala, Lutz; Norberg, Nicholas; Schaltegger, Urs; Schoene, Blair; Tubrett, M. N.; Whitehous, M. J., 2018, Plešovice zircon—A new natural reference material for U-Pb and Hf isotopic microanalysis: Chemical Geology, v. 249, no. 1-2, p. 1–35. [https://doi.org/10.1016/j.chemgeo.2007.11.005]

Tabor, R. W.; Waitt, R. B., Jr.; Frizzell, V. A., Jr.; Swanson, D. A.; Byerly, G. R.; Bentley, R. D., 1982, Geologic map of the Wenatchee 1:100,000 quadrangle, central Washington: U.S. Geological Survey Miscellaneous Investigations Series Map I-1311, 1 sheet, scale 1:100,000, with 26 p. text. [https://doi.org/10.3133/i1311]

Telford, W. M.; Geldart, L. O.; and Sheriff, R. E., 1990, Applied Geophysics: New York, Cambridge University Press, 770 p.

UNAVCO, 2008, Yakima 2008 project, collected on Apr. 26, 2008 by NCALM, 3-ft resolution, accessed Aug. 31, 2020 [http://lidarportal.dnr.wa.gov/], metadata available on portal [ger_yakima_2008_lidar_project_report.pdf].

Vaccaro, J. J.; Jones, M. A.; Ely, D. M.; Keys, M. E.; Olsen, T. D.; Welch, W. B.; Cox, S. E., 2009, Hydrogeologic framework of the Yakima River basin aquifer system, Washington: U.S. Geological Survey Scientific Investigations Report 2009-5152, 106 p., 4 plates. [http://pubs.usgs.gov/sir/2009/5152/]

WA DNR, 2014, Colockum 2014 project, collected between Jun. 25 and Jul. 6, 2014 by Geoterra, Inc., 3-ft resolution, accessed Aug. 31, 2020 [http://lidarportal.dnr.wa.gov/], metadata available on portal [ger_colockum_2014_lidar_report.pdf].

WA DNR, 2018a, Yakima Basin 2018 project, collected between Nov. 17 and Nov. 25, 2017 and May 8 and May 23, 2018 by Quantum Spatial, Inc., 3-ft resolution, accessed Aug. 31, 2020 [http://lidarportal.dnr.wa.gov/], metadata available on portal [ger_yakima_basin_2018_lidar_report.pdf].

WA DNR, 2018b, Yakima Basin North 2018 project, collected between Jul. 24 and Sep. 2, 2018 by Quantum Spatial, Inc., 3-ft resolution, accessed Aug. 31, 2020 [http://lidarportal.dnr.wa.gov/], metadata available on portal [ger_yakima_basin_north_2018_lidar_report.pdf].

Wallinga, Jakob; Murray, Andrew; Wintle, Ann, 2000, The single-aliquot regenerative-dose (SAR) protocol applied to coarse-grain feldspar: Radiation Measurements, v. 32, no. 5–6, p. 529–533. [https://doi.org/10.1016/S1350-4487(00)00091-3]

Waitt, R. B., Jr., 1979, Late Cenozoic deposits, landforms, stratigraphy, and tectonism in Kittitas Valley, Washington: U.S. Geological Survey Professional Paper 1127, 18 p. [https://doi.org/10.3133/pp1127]

Wells, R. E.; McCaffrey, Robert, 2013, Steady rotation of the Cascade arc: Geology, v. 41, no. 9, p. 1027–1030. [https://doi.org/10.1130/G34514.1]

Wells, R. E.; Weaver, C. S.; Blakely, R. J., 1998, Fore-arc migration in Cascadia and its neotectonic significance: Geology, v. 26, no. 8, p. 759–762. [https://doi.org/10.1130/0091-7613(1998)026<0759:FAMICA>2.3.CO;2]

Williams, Howel; Masson, P. H., 1949, Geology of the Macdoel quadrangle and circular soil structures in northeastern California: California Division of Mines and Geology, Bulletin 151, scale 1:125,000. [https://ngmdb.usgs.gov/Prodesc/proddesc_531.htm]

Wilson, M. S.; Dyman, T. S.; Condon, S. M., 2008, Evaluation of well-test results and the potential for basin-center gas in the Columbia basin, central Washington. *In* U.S. Geological Survey eastern Oregon and Washington Province Assessment Team, Geologic assessment of undiscovered gas resources of the eastern Oregon and Washington province: U.S. Geological Survey Digital Data Series DDS–69–O, ch. 4, 12 p. [https://pubs.usgs.gov/dds/dds-069/dds-069-o/REPORTS/69_O_CH_4.pdf]

Wolff, J. A.; Martin, B. S.; Tolan, T. L.; Wells, R. E., editors, The Columbia River flood basalt province: Geological Society of America Special Paper 497, p. 363–400. [https://doi.org/10.1130/2013.2497(15)]

Yakima Nation, 2010, Kittitas Valley Creeks 2010 project, collected on May 12 and Jun. 13, 2010 by Watershed Sciences, Inc., 3-ft resolution, accessed Aug. 31, 2020 [http://lidarportal.dnr.wa.gov/], data available on portal [ger_kittitas_valley_creeks_2010_lidar_report.pdf].

Appendix A. Fluxgate Magnetometry

The portable fluxgate magnetometer is operated according to the following field procedure: a fresh basalt specimen is collected from an outcrop where paleo-horizontal is known. A permanent marker is used to mark the top of the specimen with a negative sign ("negative side"). Then the opposite side of the specimen is marked with a positive sign ("positive side") in the direction of magnetic inclination plunging roughly 60°N through the specimen to its opposite side. This is done for at least ten test specimens ranging in size from 4–18 inches in diameter. The probe of the fluxgate magnetometer is switched on, the probe is oriented within the earth's magnetic field so the digital dial reads zero or as close to zero as possible. Zeroing the dial can be done either by careful orientation of the probe orthogonal to the earth's magnetic field or introducing a magnetic body (a hammer) to induce a zero reading. Once the dial reads zero, the positive sign is slowly and horizontally brought closer to the probe, but not touching the probe. The dial will readout a positive or negative number. The same is done for the opposite side with the negative sign. If the "positive side" yields a positive reading and the "negative side" yields a negative reading, then the sample is possibly normal polarity. The larger the dial's number, the stronger the specimen's remanent magnetic field, and the greater our confidence that the measurement was successful, particularly if the rock sample has a reversed magnetization.

Reverse readings ("positive side" yields a negative reading, and "negative side" yields a positive reading) are more reliable than normal readings. A reverse reading reflects a polarity from an ancient magnetic field that was not remagnetized. A normal reading, on the other hand, is ambiguous as it could reflect remagnetization to the modern normal polarity of Earth's magnetic field. This could occur during a post-depositional event, for example a lightning strike.

The probe sensitivity (in Tesla) of the fluxgate magnetometer used here is unknown.